Natural Resources Canada | Ressources naturelles Canada

GEOLOGICAL SURVEY OF CANADA

OPEN FILE 8018

Geological Characteristics and Petroleum Resource Assessment of the Macasty Formation, Anticosti Island, Quebec, Canada

Z. Chen, D. Lavoie, C. Jiang, M.J. Duchesne and M. Malo

2016

Canada

GEOLOGICAL SURVEY OF CANADA
OPEN FILE 8018

Geological Characteristics and Petroleum Resource Assessment of the Macasty Formation, Anticosti Island, Quebec, Canada

Z. Chen[1], D. Lavoie[2], C. Jiang[1], M.J. Duchesne[2] and M. Malo[3]

[1] Geological Survey of Canada – Calgary, Alberta
[2] Geological Survey of Canada – Québec, Québec
[3] Institut National de la Recherche Scientifique – Eau Terre Environnement, Québec, Québec

2016

doi:10.4095/297865

This publication is available for free download through GEOSCAN (http://geoscan.nrcan.gc.ca/)

Recommended citation
Chen, Z., Lavoie, D., Jiang, C., Duchesne, M.J., and Malo, M., 2016. Geological Characteristics and Petroleum Resource Assessment of the Macasty Formation, Anticosti Island, Quebec, Canada; Geological Survey of Canada, Open File 8018, 67 p. doi:10.4095/297865

Publications in this series have not been edited; they are released as submitted by the author.

Table of Contents

ABSTRACT 2
INTRODUCTION 3
GEOLOGIC SETTING 3
HYDROCARBON EXPLORATION ON ANTICOSTI ISLAND 5
DATASETS 7
THE MACASTY FORMATION 8
Structural framework 10
Mineralogy 11
Geomechanics 11
Porosity /permeability 12
Type of organic matter 20
Thermal maturation 21
PETROLEUM RESOURCE ASSESSMENT 28
Methodology 28
Thermal Maturity and Hydrocarbon Generation Models 32
Volumetric Parameter Estimation 37
Reservoir parameters 39
Assessment Results 47
DISCUSSION 52
CONCLUSIONS 55
ACKNOWLEDGEMENTS 56
REFERENCES 57

ABSTRACT

This study presents the first independent evaluation of the in place hydrocarbon resources for the Macasty Formation on Anticosti Island. The evaluation uses the dual porosity model of the GSC. The data consists of all public domain information as well as confidential data provided by the operators on the island.

Our evaluation indicates significant volume of both oil with a best estimate or P50 of 32.2 billion barrels of oil (BBO) with maximum (P5) of 55.1 and minimum (P95) of 17.4 BBO and for natural gas with a best estimate or P50 of 51.2 trillion cubic feet (TCF) with maximum (P5) of 83.4 and minimum (P95) of 29.6 TCF. However, the comparison of the maximum (55.1 BBO / 83.4 TCF) and minimum (17.4 BBO / 29.6 TCF) resources in place illustrates a significant uncertainty on the evaluation most likely related to the relative low density and variable quality of the data (spatial coverage, diverse acquisition methods).

Previous industry estimates suggest an in-place P50 resource of 42.9 billion barrels of oil equivalent, a value that lump together oil and gas based on a thermal equivalence of 1 barrel of oil equivalent for 6000 cubic feet of gas. Our P50 result is 40.6 billion of barrels of oil-equivalent. From these results, a ratio of 79% oil to 21% gas is proposed as in-place resource on the island. Because of the lack of production data, no attempt was made to evaluate the recovery portion of the in-place resource.

INTRODUCTION

The recent exploration for unconventional resources on Anticosti Island has targeted the Macasty Formation, a demonstrated hydrocarbon source rock for conventional hydrocarbon systems (Lavoie et al., 2009) but little understanding of its unconventional reservoir potential. Since 2014, the Geological Survey of Canada has initiated research projects focused on various aspects related to unconventional resources exploration and development on Anticosti Island. These include: 1) a comparative fracture analyses of the pre- and post-Taconian sedimentary successions from field and remote-sensing data (Pinet et al., 2015; Brake and Pinet, 2015), 2) well-log geomechanical analyses and characterization of the shale target and its overlying cover sequence (Séjourné, 2015a, 2015b), 3) reprocessing of reflection seismic data for a better control on the thickness of the Macasty Formation, 4) deployment in fall 2015, of three seismograph stations to record the natural seismicity on the island and 5) the compilation of organic geochemistry and well log data to carry out a detailed evaluation of the potential of in-place-oil and gas resources of the Macasty Formation. This report presents the results of the latter research project.

The studies 1, 2, 3 and 5 were carried out under the Geoscience for New Energy Supply (GNES) program with funding from the PERD (Program for Energy Research and Development) program; the seismicity project (#4 above) is part of the Environmental Geoscience Program (EGP) with funding from the ecoEII (EcoEnergy Innovation Initative) program.

GEOLOGIC SETTING

The Anticosti Basin is a large sedimentary onshore and offshore basin covering the northern part of the Gulf of St. Lawrence (Sanford, 1993; Mossop et al., 2004). The Anticosti Basin is located at the interpreted transition between the Quebec Reentrant and the St. Lawrence Promontory (Allen et al., 2009). It includes the eastern part of the St. Lawrence Platform (*sensu* Sanford, 1993), which corresponds to the Paleozoic autochthonous sedimentary cover of the north-eastern Precambrian craton in Canada.

The onshore succession of the Anticosti-Mingan islands presents several distinct characteristics compared to those of southern Quebec and western Newfoundland (Lavoie, 2008; Lavoie et al., 2012): 1) it is located farther from the Appalachian structural front and thus less deformed (Pinet et al., 2012); 2) the age of the basal sediments that unconformably overlies the Precambrian basement is significantly younger compared to southern Quebec and western Newfoundland with the lack of Cambrian to lowermost Ordovician strata (Lavoie et al., 2012) and 3) the Anticosti Basin succession is more stratigraphically continuous and lacks major tectonic-related sedimentary hiatus (Long, 2007).

In the northern part of the Anticosti Basin, the sedimentary beds dip gently (approximately 3°) toward the southwest (Pinet et al., 2015). The base of the succession is exposed in the Havre Saint-Pierre area (Fig. 1) and unconformably overlies the metamorphic rocks of the Precambrian Grenville domain.

Overall, the stratigraphic succession thickens towards the southwest. The basal strata consist of the Lower Ordovician Romaine Formation (Desrochers and James, 1988; Desrochers et al., 2012) which corresponds to a 400-800 m thick peritidal-dominated, limestone and dolostone assemblage recording high-frequency cyclic sedimentation on a passive margin. The Romaine Formation belongs to the continental-wide passive margin deposits known as the "Great American Carbonate Bank" of Wilson et al. (1991). Along the north shore of the Gulf of St. Lawrence and on the Mingan islands, this lower succession is unconformably overlain by a 400-600 m thick Taconian shallow marine foreland basin succession in which basal siliciclastics were succeeded by predominantly shallow, open marine carbonates (Middle Ordovician Mingan Formation; Desrochers, 1988). The overlying Upper Ordovician Macasty Formation forms part of the seafloor bedrock between Mingan and Anticosti islands. It is not exposed onshore, but the formation has been encountered in all hydrocarbon exploration wells drilled on Anticosti Island with the exception of the Sandtop well (D010, Fig. 1) at the eastern end of the island. It corresponds to a 0 to 125 m thick interval of dark marine and organic-rich limy shale that is presently the main focus of resource play hydrocarbon exploration in the area. Overlying units are exposed on Anticosti Island and include: 1) a 900-1200 m thick Upper Ordovician siltstone-dominated interval overlain by outer ramp shallowing-upward carbonates (Vauréal Formation) with complex facies zonation (Achab et al., 2011); 2) a *circa* 60 m thick subtidal carbonates (Ellis Bay Formation) with local microbial-metazoan bioherms (Desrochers et al., 2010) and 3) the 400 m thick Anticosti Group (Becsie, Merrimack, Gun River, Jupiter and Chicotte formations) that regroups various carbonate facies with minor siliciclastics deposited on a storm-dominated carbonate ramp (Sami and Desrochers, 1992; Desrochers, 2006). Offshore, south and southwest of Anticosti Island, approximately 1140 m of younger sedimentary units complete the preserved Anticosti Basin succession (Pinet et al., 2012).

On Anticosti-Mingan islands, the exposed sedimentary succession is weakly deformed, affected by only minor structural features (fractures, minor faults) that record the distant foreland strain associated with Appalachian orogenesis and younger events (Bordet et al., 2010; Pinet et al., 2015). Seismic interpretation on Anticosti Island indicates that the base of the sedimentary succession is affected by steeply-dipping normal faults (including the Jupiter Fault; Fig. 1) that do not extend into the Silurian units (Lynch, 2001; Castonguay et al., 2005; Bordet et al., 2010). Significant downthrown movement and thickening of sedimentary successions is recorded on the southwest side of the Jupiter Fault. South of Anticosti Island, the offshore part of the basin includes a 40 km wide fold-and-fault belt oriented sub-parallel to the coastline of the Gaspé Peninsula. The structural style of the offshore domain is characterized by broad open synclines, narrow anticlines and NW-striking faults with dextral strike separations (Pinet et al., 2012).

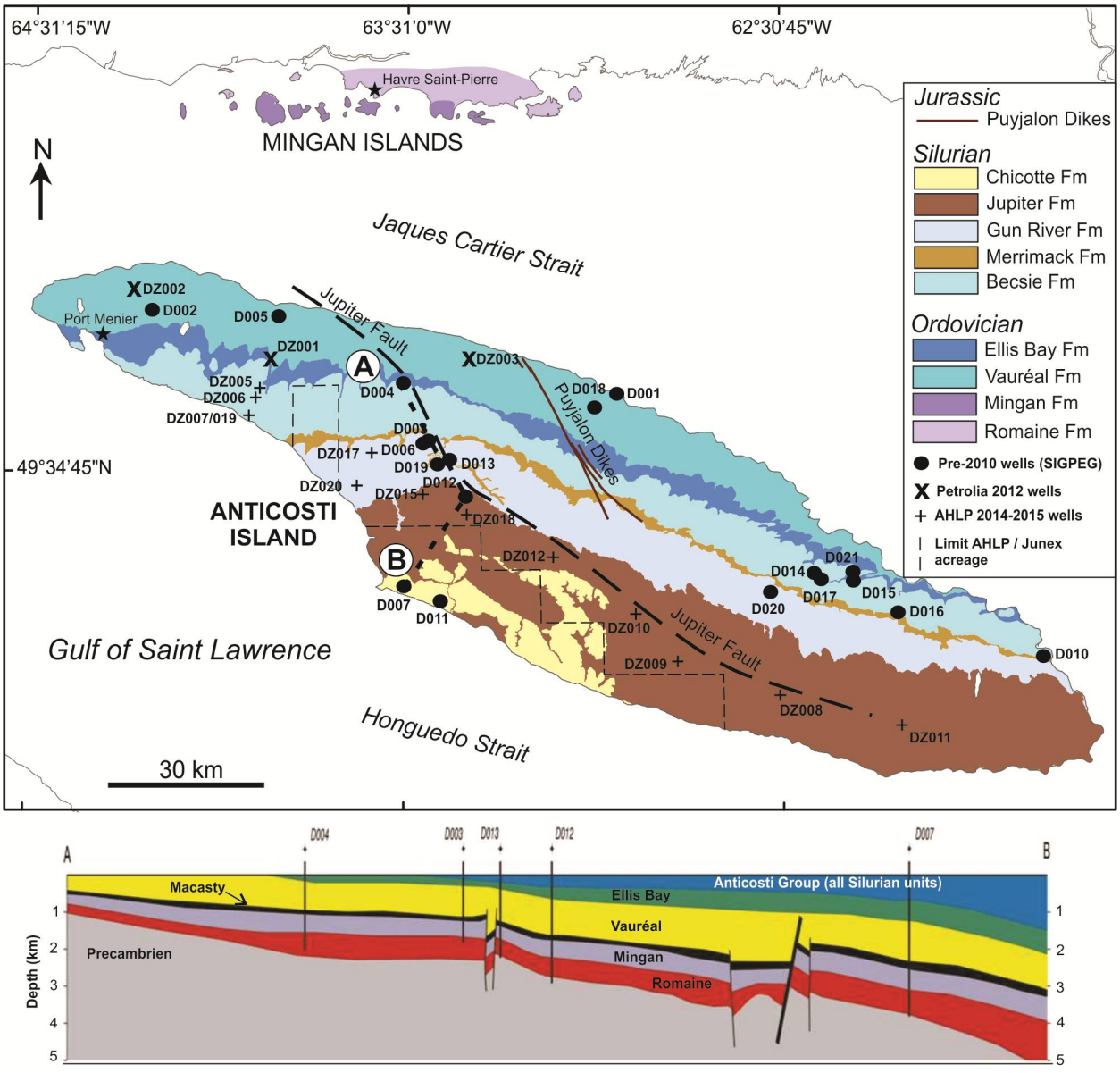

Figure 1. Geological map of Mingan and Anticosti islands with the location of the 21 conventional exploration wells (D001 to D021), the 3 Petrolia 2012 core holes and the 12 Anticosti Hydrocarbon L.P. 2014-2015 cores. The Macasty Formation does not outcrop onshore. Lower; a schematic N-S cross-section (A – B) on Anticosti Island based on seismic profiles (Lynch, 2001) and well data. Extensional faults only affect the Ordovician succession and do not extend in the Silurian strata. The Macasty Formation is progressively thicker and deeper towards the south – southwest. Modified from Lavoie et al. (2009), geology extracted from the Sigeom database (Ministère des Ressources Naturelles du Québec), August 2014 and the position of the Jupiter Fault (black broken line) is from Bédard et al. (2014).

HYDROCARBON EXPLORATION ON ANTICOSTI ISLAND

Hydrocarbon exploration of Anticosti Island started in 1962 with the drilling of the Lowlands Gamache Princeton Lake (D002) and New Associated Con-Paper (D003) wells (Fig. 1) (*N.B.* the Lowlands Gamache Carleton Point D001 well was drilled in 1963). Over the next 50 years, exploration

was cyclic with episodic periods of seismic acquisition and drilling for conventional exploration targets; during the first exploration period on Anticosti, twenty-one (21) wells were drilled at various localities dispersed all over the island (Fig. 1). Bertrand (1987) suggested that the Upper Ordovician Macasty Formation is an excellent hydrocarbon source rock with significant generation potential and that the thermal maturation of the formation ranges from the oil window in the northeast domain of the island to the condensate / dry gas windows, southeast of the Jupiter Fault. Various hydrocarbon play concepts were tested by diverse operators including diagenetic closure along the post-Romaine unconformity and structural closure along synsedimentary faults but these plays were not successful (Lynch, 2001; Lavoie et al., 2009; Dietrich et al., 2011). Petrographic and geochemical attributes combined with other geophysical evidence support the hypothesis that Lower and Upper Ordovician carbonates of Anticosti Island were hydrothermally altered and form porous dolostone reservoirs in fault-bounded seismic sags (Lavoie et al. 2005; Lavoie and Chi, 2010). Drilling for conventional plays on the island resulted in the recognition of locally significant porosity in this structural-diagenetic play but no economic accumulation of oil or gas. This hydrothermal dolomite play is still considered as a potential exploration target on the island.

In 2010, a new exploration paradigm was developed on Anticosti Island considering the Macasty Formation as a resource play. The time and facies equivalent Utica / Point Pleasant in Ohio had been producing natural gas and condensates for a couple of years at that time. In 2011, based on previous public domain and new proprietary exploration data, Sproule Associates and Netherland, Sewell & Associates (NSAI) produced resource evaluations for the acreage held by Petrolia/Corridor Resources and by Junex, respectively. The evaluation for the Pétrolia/Corridor Resources acreage (which covers about 77% of the island) suggested an in-place resource of 30.7 BBoe (Billions of barrels of oil equivalent) at P50; whereas the Junex acreage (around 16% of the island) was interpreted to hold 12 BBoe at P50 (all oil from NSAI report). The Junex acreages are located in the southwestern most region of the island (Fig. 1), in the area where the Macasty is deeper and most likely more thermally mature. From 2012 to 2015, sixteen (16) stratigraphic holes were drilled on Anticosti Hydrocarbons L.P. consortium (Pétrolia - Corridor Resources - Saint-Aubin E&P - Resource Québec) acreage to gather cores of the Macasty Formation for thermal and geochemical characterization of the shales (Fig. 1). Table 1 identifies and locates the wells covered by our study as well as the depths of the top and the base of the Macasty Formation, therefore its gross thickness, as well its net thickness for our study (hydrocarbon saturation > 60% with a minimum of saturated pores of 2%; see further)

Anticosti Island covers about 7900km^2, a total of 37 wells were drilled on the island since 1962 resulting in an average of 1 exploration well for every 200 km^2. Such a low well density for hydrocarbon

exploration is typical for frontier sedimentary basins, moreover, the density of samples, types of physical and geochemical and the nature of well-logs vary significantly between the pre and post-2010 wells.

Well #	Name	Latitude	Longitude	Macasty top (m)	Mingan top (m)	Gross Thickness (m)	Net thickness (m)
D001	Lowland Gamache Carleton Point #1	49° 42' 30.2"	62° 55' 57"	398	440.4	42.4	N/A
D002	Lowland Gamamche Princeton Lake # 1	49° 52' 8.9"	64° 12' 15.9"	911.4	983.6	72.2	N/A
D003	New Associated Consolidated Pape r#1	49° 37' 20.2"	63° 26' 17.5"	1191.2	1204	12.8	N/A
D004	Lowlands Gamache, Oil River # 1	49° 44' 30,2	63° 30' 42,5"	1011.9	1030.2	18.3	N/A
D005	Lowlands Gamache High Cliff # 1	49° 51' 30.2"	63° 52' 7.6"	847.3	885.4	38.1	9
D006	New Associated, Jupiter Anticosti # 1	49° 37' 15,2"	63° 26' 22,5"			N/A	N/A
D007	Atlantic Richfield Company (ARCO) # 1	49° 23' 19.2"	63° 31' 27.4"	2405.0	2487.0	82.0	50
D012	Shell Encal Corridor Anticosti Roliff #1	49° 32 23.2"	63° 21' 0.1"	1640.0	1698.0	58.0	35
D013	Shell Encal Corridor Anticosti Jupiter #1	49° 35' 36.2"	63° 25' 0.5"	1235.0	1253.0	18.0	15
D014	Shell Encal Corridor Anticosti Chaloupe #1	49° 23' 39.5"	62° 26' 49.4"	878.0	918.0	40.0	20
D015	Shell Encal Corridor Anticosti Saumon #1	49° 23' 39.4"	62° 22' 06.3"	850.0	885.0	35.0	15
D016	Shell Encal Corridor Anticosti Dauphine #1	49° 20' 17.9"	62° 14' 11.9"	904.0	919.0	15.0	5
D017	Corridor / Hydro-Québec Anticosti Chaloupe # 1	49° 23' 41,8"	62° 26' 05,4"	898.0	925.0	27.0	N/A
D018	Hydro-Québec/Corridor Anticosti, MacDonald # 1	49° 42' 02,5"	62° 59' 55,9"	527.0	568.0	41.0	34
D019	Corridor / Hydro-Québec Anticosti Jupiter # 1	49° 35' 33,2"	63° 25' 1,9"	1300.0	1325.0	25.0	N/A
D020	Pétrolia / Corridor Anticosti Chaloupe No.1	49° 22' 3,9"	62° 32' 25,5"	1021.0	1086.0	40.0	30
D021	Corridor / Pétrolia Anticosti Saumon No. 1	49° 23' 46,1	62° 22' 30,1"			N/A	N/A
DZ001	Pétrolia Sondage No 2, HighCliff	49° 46' 43.9"	63° 52' 59.6"	1132	1189	57	N/A
DZ002	Pétrolia Sondage No 4, Princeton Lake	49° 53' 38"	64° 15' 57.6"	850	941.5	91.5	N/A
DZ003	Pétrolia, Sondage No 1, Oil River	49° 46' 16.1"	63° 21' 5.1"	577.5	606.5	29	N/A
DZ005	Hydrocarbures Anticosti SEC, Sainte-Marie # 1	49° 45' 19.96''	63° 52' 59.52''	1175.5	1237.5	62	45
DZ006	Hydrocarbures Anticosti SEC, Caribou # 1	49° 43' 27.15''	63° 54' 30.06''	1432.6	1523.2	90.6	74
DZ007	Hydrocarbures Anticosti SEC, Canard # 1	49° 40' 58.88''	63° 54' 52.18''			N/A	N/A
DZ008	Hydrocarbures Anticosti SEC, Cerf-Sau # 1	49° 14' 15.24''	62° 28' 48.11''	1204	1245	41	25
DZ009	Hydrocarbures Anticosti SEC, Martin-la-Mer # 1	49° 17' 00.90''	63° 47' 45.67''	1452.5	1507.5	55	45
DZ010	Hydrocarbures Anticosti SEC, Lac-Martin # 1	49° 21' 29.65''	62° 52' 33.86''	1280	1310.5	30.5	24
DZ011	Hydrocarbures Anticosti SEC, Bell # 1	49° 09' 14.90''	62° 12' 05.36''	1206.5	1220	13.5	0.5
DZ012	Hydrocarbures Anticosti SEC, Chicotte # 1	49° 26' 57.90''	63° 08' 39.45''	1631	1698.5	67.5	41
DZ015	Hydrocarbures Anticosti SEC, Jupiter-South # 1	49° 34' 35.13''	63° 26' 03.34''	1571.5	1657.5	86	46
DZ017	Hydrocarbures Anticosti SEC, NACP West # 1	49° 38' 36.46''	63° 33' 27.04''	1397	1433.9	36.9	34
DZ018	Hydrocarbures Anticosti SEC, Roliff-Graben # 1	49° 32' 39.95''	63° 20' 40.00''	1674.7	1779.8	105.1	94
DZ019	Hydrocarbures Anticosti SEC, Canard # 2	49° 40' 59.02''	63° 54' 52.18''	1544.4	1644	99.6	70
DZ020	Hydrocarbures Anticosti SEC, La Loutre # 1	49° 35' 17.76''	63° 38' 13.53''	1691.25	1735.25	44	38

Table 1. Public domain (D) and confidential (DZ) wells evaluated in this study. The table also shows the depth interval of the Macasty Formation and its resulting gross and net (hydrocarbon saturation > 60% with a minimum of hydrocarbon saturated pores of 2%) thickness. Not all wells have logs for evaluating net thickness. N/A not available

DATASETS

As part of this research project, various data sharing agreements were concluded with the consortium Anticosti Hydrocarbons L.P. (AHLP: Petrolia – Corridor Resources – Saint-Aubin E&P – Ressources Québec) and Junex Exploration providing to the GSC research group unrestricted access to all confidential 2012 geoscience data on Anticosti island. Other agreements were reached with the Ministère

de l'énergie et des ressources naturelles du Québec for the use of all public well-log data hosted in their database (SIGPEG) and access to AHLP core hole programs of 2014-2015.

In order to carry out this study of the quantitative evaluation of the in-place resources in the Macasty Formation, we have used various datasets.

Rock-Eval - Lavoie et al. (2011) contains 50 public domain Rock Eval data, data from Pétrolia and AHLP consist of 711 Rock Eval analyses, Junex Exploration dataset for D007 consist of 7 Rock Eval data from the D007 well.

Organic matter reflectance – AHLP dataset consist of 190 $\%VR_{equiv}$ from the Petrolia 2012 core holes, Junex Exploration dataset consist of 2 values of $\%VR_{equiv}$ from D007 well.

Digital well logs – Digital logs from 17 public domain wells and 12 core holes 2014-2015 from AHLP. A total of 21 wells were selected for the log-based evaluation from available suite of logs (Table 1)

Porosity – Permeability – 399 analyses from the 3 Petrolia 2012 and the 12 AHLP 2014-2015 core holes.

X-Ray Diffraction – 348 analyses from 3 Petrolia 2012 and the 12 AHLP 2014-2015 core holes.

THE MACASTY FORMATION

This section presents a summary of our current understanding of the geology and geochemistry of the Macasty Formation; data presented here are used in the resource evaluation of the in-place resources. The description of the Macasty Formation is based on well data, including the lithological description of well cuttings and cores, the geochemical analyses (Rock Eval), petrographic description and available well-logs data. To the contrary of its stratigraphic equivalent in southern Quebec (Utica Shale), the Macasty Formation does not outcrop anywhere.

Stratigraphy and thickness

The Macasty Formation has a fairly uniform lithologic composition; it consists of siliceous, slightly calcareous black shale and subordinate calcareous siltstone, locally rich in graptolites. At places, some intervals of intraformational limestone conglomerates are described, with clast being derived from the underlying Mingan Formation (Bertrand, 1987). Based on graptolite faunas and well logs, the transition with the underlying carbonates of the Mingan Formation is sharp and locally described or interpreted as disconformable (Riva, 1969; Lynch, 2001). Moreover, Riva (1969), based on graptolite fauna, has proposed the presence of another disconformity a few metres above the base of the formation. The Macasty Formation is conformably overlain by the Vauréal Formation. The lower interval of the Vauréal Formation was previously known as the English Head Formation (Schuchert and Twenhofel,

1910), a term now abandoned. The contact is put at the base of the first limestone bed in a succession of grey to greenish limestones with surbordinate green and gray shales.

The age of the Macasty Formation is based on its abundant graptolite fauna (Riva, 1969), it was interpreted to be "Trentonian – Maysvillian" from the old North American stratigraphic chronostratigraphic scheme. The current stratigraphic chart for the Ordovician translates to the lower to middle part of the Katian stage (Upper Ordovician).

The Macasty Formation has been encountered in all exploration holes drilled on Anticosti Island excluding in the Sandtop well (D010) and thus it is assumed to be present everywhere except for the eastern end of the island. The thickness of the succession is however, variable (Séjourné and Malo, 2015; their Fig. 36 and Fig. 2 herein). Table 1 presents the thickness of the Macasty Formation based on previous interpretations and those adjusted from recent well-logs analyses (Séjourné, 2015 a, b and this study). The exploration wells drilled to the north-east of the Jupiter Fault indicate that the unit varies in thickness from seemingly absent at the eastern end of the island (Sandtop well, D010; Table 1) to a maximum of 40 m (Chaloupe well, D020, Table 1). Based on well and seismic information, the thickness of the Macasty north-east of the Jupiter Fault is thickest in the north-east central part of the area (Fig. 2), between the MacDonald (D018; Table 1) and Chaloupe (D020; Table 1) wells. The exploration wells drilled south-west of the Jupiter Fault indicate that the unit thickens towards the west and southwest. The indicated thickness of the unit range between 12 m (NACP D003 well; Fig. 2 and Table 1) to a maximum of 105 m (Roliff graben DZ018 well; Fig. 2 and Table 1); based on seismic interpretation the thickest accumulation of the Macasty Formation is around 125 m at the extreme west tip of the island. From well and seismic information, the Macasty Formation south-west of the Jupiter fault has two areas with thicker accumulations, one at the western end of the island (e.g., D002, DZ002, DZ006 and DZ012 wells, Fig. 2 and Table 1) and a second one in the south-west central area (D007, DZ015, DZ018 wells, Fig. 2 and Table 1).

The top of the Macasty Formation in the subsurface is progressively deeper from the northeast to the southwest from 350 meters (D001 well, Fig. 2 and Table 1) down to 2405 meters (D007 well, Fig. 2 and Table 1) with a rapid drop in the area south of the Jupiter Fault (Table 1 and Fig. 1).

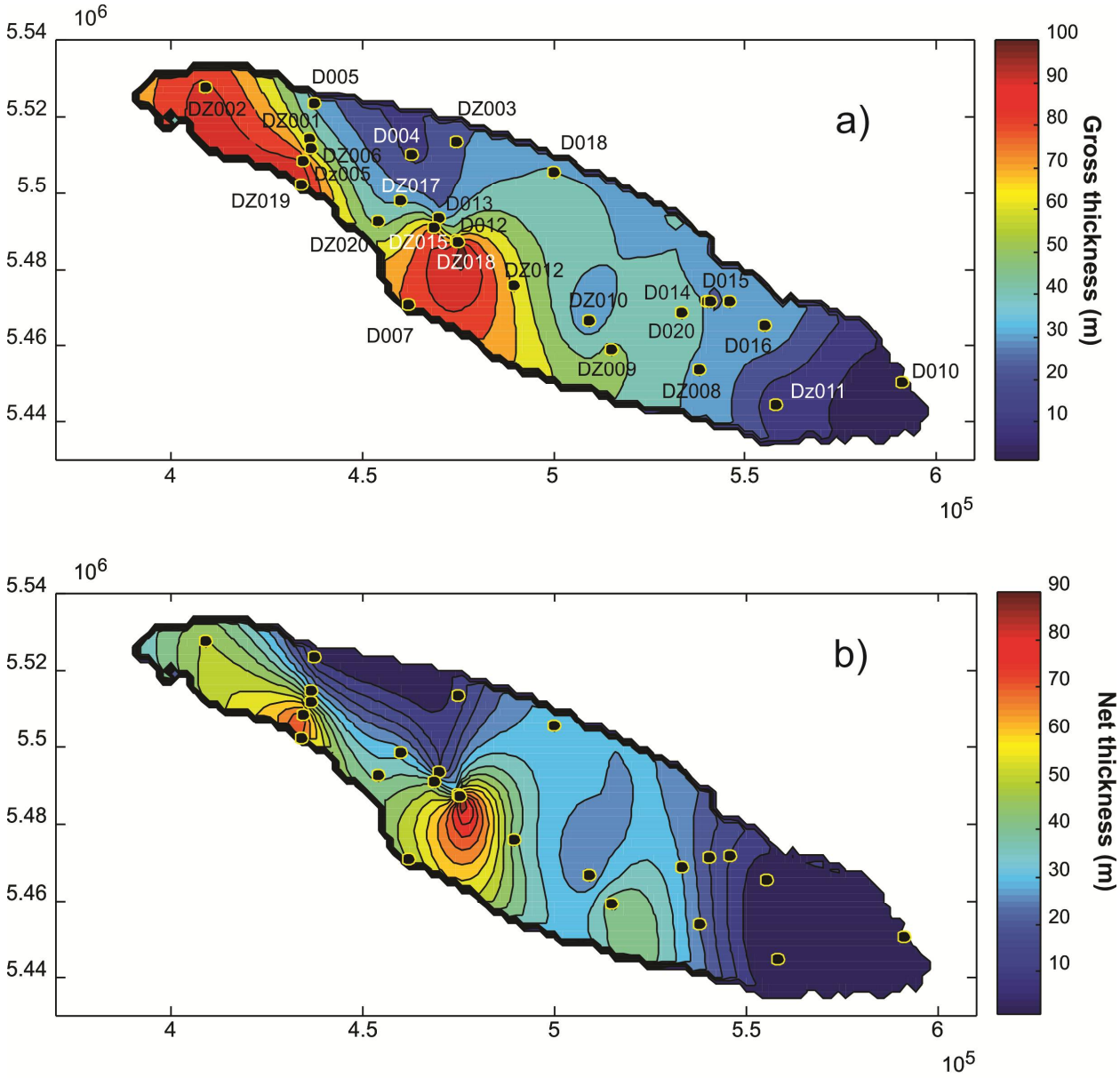

Figure 2. Krigged map of gross (a) and net (b) thickness map (in meters) of the Macasty Formation. Data in Table 1. Longitude (UTM) along horizontal axis; latitude (UTM) along vertical axis.

Structural framework

The Macasty Formation does not outcrop onshore (Mingan and Anticosti Islands) and our current understanding of the deformation of the sedimentary succession relies on observations from underlying and overlying successions on Mingan and Anticosti islands, respectively. Pinet et al. (2015) carried out a detailed outcrop-based structural analysis of the pre- (Lower to Middle Ordovician) and post-Macasty (uppermost Ordovician and lower Silurian) successions that temporally correlate with the pre-, syn and post-Taconian orogenic event elsewhere in the northeastern Appalachians.

Fractures and joints dissect nearly flat-lying Lower Ordovician to lower Silurian strata. Fracture mapping on the Mingan Islands and on Anticosti Island indicates that the two predominant joint sets are nearly orthogonal and trend ~ N100° and ~N10°. In most cases, the ~N100° joints are the most continuous, suggesting that they form a systematic set of fractures that likely extend to a significant depth. The spacing of the ~N100° joint set is partly controlled by the mechanical characteristics of the fractured bed, with some variations (continuity, patterns) clearly linked to the more or less argillaceous nature and bed thickness of the dominant limestone facies. Some joints exhibit significant horizontal and vertical continuity and are locally concentrated in structural corridors, suggesting that they may influence subsurface fluid flow if open at depth.

In the study area, the ~N100° systematic joint set, present in the Ordovician and Silurian successions is approximately parallel with the deformation front documented south of Anticosti Island (Pinet et al., 2012), suggesting that it formed through extension in a forebulge setting. Consequently, these systematic joints would be contemporaneous with the Middle-Late Devonian Acadian orogeny that caused significant crustal thickening in the northern Appalachians. The Ordovician part of the Anticosti Basin sedimentary succession is partly contemporaneous with the Taconian orogeny, but the far-field effects of this deformation event are unclear.

Mineralogy

The shales of the Macasty Formation are less calcareous compared to those of the Utica Shale in southern Quebec (Chen et al., 2014; Lavoie et al., 2014). X-Ray diffraction analyses (348) of the shales of the Macasty Formation (Table 2) suggest that the average carbonate (calcite + dolomite) content reaches 21% compared to 58% in the Utica Shale. The silica content (quartz + feldspars) averages 44% compared to less than 16% for the Utica Shale. However, the clay content is fairly similar for both units (30 and 24% for the Macasty and Utica shales, respectively). Therefore, as a whole, the Macasty has a dominant content of brittle minerals that compares well to that of the Utica Shale (70% versus 76%, respectively), although not dominated by the same components.

Unit	# analyses	Quartz	Feldspars	Carbonates	Pyrite	Clays
Macasty	348	36%	8%	21%	5%	30%
Upper Utica	90	14%	5%	60%	1%	20%
Lower Utica	120	11%	4%	57%	2%	26%
Utica average	210	12%	4%	58%	2%	24%

Table 2: Comparative mineralogy of the Macasty and Utica shales. The Utica Shale data is from Thériault (2012).

Geomechanics

The log-based geomechanical studies (Séjourné, 2015a; 2015b) documented the mechanical properties of the Macasty Formation and its cover sequence over Anticosti Island. The Petrolia / Corridor

Anticosti Chaloupe No. 1 well (D020) was the only well with available acoustic S wave log available at the time of our study. This well was used to generate a synthetic acoustic wave. A series of calibration tests were therefore carried out to determine the best method to generate a synthetic acoustic wave for each of the analyzed wells. Based on the available regional data and parameters necessary for calibration, eight (8) well logs were selected for the regional geomechanical study.

The presence of net mechanical contrasts between Macasty Formation and the overlying and underlying units was demonstrated. These mechanical contrasts result in the presence of barriers to propagation of hydraulic fractures outside the Macasty Formation. The Macasty is more brittle than the overlying clay-rich Vauréal Formation and less brittle than the underlying carbonates of the Mingan Formation.

Regionally the results show a remarkable homogeneity from one well to another, except in the south-central part of the island where the mechanical contrast is present higher up in the cover sequence in well D007 rather than immediately above the Macasty Formation. In this case the phenomenon may be real or an artifact linked to the methodological limitations of the study (Séjourné, 2015a; 2015b), it is not possible to decide on the basis of currently available data.

Porosity /permeability

Effective and hydrocarbon-filled porosities and permeability measurements on the shales of the Macasty Formation were performed on 399 samples at various service laboratories. Table 3 summarizes the results.

		Hydrocarbon filled porosity (% BV)		Effective porosity (% BV)		Pressure-Decay permeability (mD)	
Wells	# analyses	Mean	Maximum	Mean	Maximum	Mean	Maximum
D020	23	2.23	2.7	2.68	3.51	0.000479	0.000739
DZ001	12	4.01	6.07	4.8	6.93	0.000167	0.000263
DZ002	19	3.3	4.88	3.67	5.23	0.000138	0.000280
DZ003	9	2.11	2.72	3.09	4.42	0.000110	0.000178
DZ005	25	2.94	4.37	3.74	4.81	0.000121	0.000211
DZ006	37	3.4	5.54	4.29	6.24	0.000158	0.000279
DZ008	17	1.43	2.15	2.14	2.49	0.000066	0.000081
DZ009	22	1.89	3.48	2.49	3.31	0.000098	0.000155
DZ010	25	1.94	2.73	2.9	3.71	0.000092	0.000142
DZ011	13	1.34	1.81	2.25	2.73	0.00006	0.000083
DZ012	34	2.21	4.28	2.72	4.73	0.000105	0.000240
DZ015	25	3.52	5.37	4.21	5.75	0.000175	0.000284
DZ017	34	3.55	5.53	4.12	6.01	0.000187	0.000314
DZ018	40	3.12	5.05	3.52	5.41	0.000161	0.000265
DZ019	34	4.16	6.64	5.41	7.59	0.000181	0.000293
DZ020	30	4.12	5.77	4.89	7.65	0.0002	0.000323

Table 3. Summary of porosity and permeability data for the shales of the Macasty Formation from 4 wells. Data provided by Anticosti Hydrocarbon L.P. consortium. B.V. is bulk volume, mD is milliDarcy.

In comparison, based on 20 samples, the Talisman Energy Saint-Edouard #1 well drilled in 2010 in the Utica Shale of southern Quebec has hydrocarbon-filled porosity between 1.23 to 2.51% of bulk volume, effective porosity ranging from 1.84 to 3.83% of bulk volume and pressure-decay permeability between 0.000132 to 0.000242 mD. The Talisman Energy Saint-Edouard #1 well had the best initial and 30 day stabilized production testing (11 mmscf/day and 6 mmscf/day, respectively) of the 28 wells drilled in the Utica Shale.

Organic geochemistry

The geochemical data are presented in Table 4 and discussed in the following sections. The DZ001 to DZ003 core holes were sampled every 50 centimeters, the DZ005 to 20 at every 1 to 2 m, the Chaloupe #1 was sampled every 3 meters, the wells in Lavoie et al (2011) were sampled at an average of every 5 meters whereas the Arco well (D007) was sampled at an average of 12 meters.

Total Organic Carbon

The potential and quality of hydrocarbon source rocks are commonly evaluated by their content of organic matter or Total Organic Carbon (TOC). The TOC value is provided by Rock Eval analysis. It is commonly accepted that a TOC value of less than 0.5wt% indicates no active source rock potential, although the evaluation of its past potential (initial TOC; iTOC) needs to be known in order to understand the original source rock potential. Table 4 presents the summary of TOC values from 10 wells reported in Lavoie et al. (2011), those from the 4 wells of Hydrocarbon Anticosti L.P. and the new D007 results from Junex. As source rocks are progressively buried and organic matter transformed into hydrocarbons, the amount of TOC is reduced.

Figure 3 and table 5 present the variation of TOC with respect to Tmax (maximum temperature for the S2 peak) commonly considered as a good indicator of thermal maturation. As expected the highest TOC value (5.5wt%, D001 well) is associated with the lowest Tmax value of our dataset (435°C), and conversely the lowest TOC value (1.9wt%, D013) correlates with a higher Tmax value (443°C). A slight negative correlation is developed between TOC and Tmax (Fig. 3), the reduction of TOC content in the Macasty Formation is rapid with a relatively slight increase in Tmax which would suggest a rapid transformation of kerogen into hydrocarbons. However, it is unknown if the wells had all a relatively similar iTOC or if local variations of organic matter content should be considered.

Well Data source	analyses	TOC (wt %)	S1 mg HC/g rock	S2 mg HC/ g rock	Tmax (°C)	HI mg HC / g TOC	OI mg CO2 / g TOC	PI S1/(S1+S2)
D007	7							
Average		2.60	1.09	0.82	456	31	21	0.58
Low		1.16	0.44	0.31	454	40	14	0.53
High		3.72	1.65	1.48	457	24	36	0.60
D020	19							
Average		3.69	3.81	20.84	442	562	18	0.16
Low		1.90	1.65	9.65	431	496	9	0.10
High		5.74	6.00	32.95	450	630	37	0.27
DZ001	111							
Average		3.99	3.20	12.89	442	319	6	0.20
Low		0.65	0.33	1.27	408	169	2	0.15
High		7.06	6.09	24.27	447	446	31	0.30
DZ002	183							
Average		4.02	4.48	11.71	441	288	9	0.29
Low		0.37	0.62	1.87	309	225	3	0.18
High		7.52	7.02	24.34	447	429	65	0.41
DZ003	55							
Average		4.00	2.21	19.43	445	482	10	0.10
Low		2.01	1.03	8.84	442	387	4	0.06
High		6.23	3.44	33.12	447	535	33	0.14
DZ005	26							
Average		4.03	3.82	10.85	436	267	8	0.26
Low		2.86	2.73	7.33	432	230	4	0.22
High		6.37	5.98	17.38	440	295	15	0.31
DZ006	38							
Average		3.63	2.69	8.68	444	237	6	0.24
Low		2.02	1.58	4,51	438	221	3	0.19
High		6.22	4.10	16,76	448	270	12	0.28
DZ008	17							
Average		3.83	2.96	16.64	441	435	2	0.15
Low		2.50	1.74	10.41	438	387	1	0.09
High		5.75	3.97	22.27	444	490	4	0.18
DZ009	22							
Average		3.94	1.97	13.69	444	346	5	0.13
Low		2.62	1.26	8.95	439	308	3	0.11
High		5.27	3.02	19.19	446	387	7	0.18
DZ010	25							
Average		3.98	3.04	15.83	443	394	5	0.16
Low		1.17	1.12	3.95	439	338	1	0.14
High		5.77	4.46	24.49	446	431	20	0.22

Well Data source	analyses	TOC (wt %)	S1 mg HC/g rock	S2 mg HC/ g rock	Tmax (°C)	HI mg HC / g TOC	OI mg CO2 / g TOC	PI S1/(S1+S2)
DZ011	13							
Average		2.69	1.97	8.67	442	323	8	0.19
Low		0.96	1.02	7.47	440	290	1	0.11
High		3.71	2.40	11.60	444	333	25	0.24
DZ012	35							
Average		4.37	2.82	11.38	445	261	5	0.20
Low		2.48	1.19	5.46	436	163	2	0.17
High		7.38	4.16	17.58	452	320	13	0.27
DZ015	35							
Average		4.02	3.46	10.60	442	260	4	0.25
Low		1.15	0.88	2.30	436	186	1	0.20
High		6.18	4.57	17.04	447	287	24	0.32
DZ017	34							
Average		4.44	2.93	12.49	444	280	4	0.19
Low		2.25	1.65	5.64	439	251	2	0.15
High		7.05	4.25	20.28	448	309	8	0.23
DZ018	40							
Average		4.06	2.41	10.24	445	251	4	0.19
Low		0.93	0.70	1.86	427	200	2	0.15
High		6.07	3.42	16.18	458	288	10	0.27
DZ019	35							
Average		3.46	2.56	6.77	442	195	5	0.27
Low		0.16	0.06	0.31	437	174	0	0.16
High		6.18	4.38	12.76	450	212	9	0.32
DZ020	30							
Average		3.60	2.29	6.33	442	175	8	0.27
Low		2.10	0.94	2.35	431	141	4	0.23
High		5.87	3.85	6.55	454	220	16	0.33
Lavoie et al. (2011)	50							
Average		3.43	1.91	11.90	439	344	12	0.12
Low		0.81	0.01	1.10	432	28	5	0.10
High		5.70	6.37	27.48	445	485	26	0.22

Table 4. Summary of Rock Eval results. TOC is Total Organic Carbon, S1 is volatiles in the rock, S2 remaining pyrolisable organic matter, Tmax is temperature of peak of S2 generation in the pyrolysis experiment, HI is hydrogen index, OI is oxygen index, PI is production index. DZ001 to DZ020 and Chaloupe #1 are from Anticosti Hydrocarbons L.P. and D007 is new results from Junex Exploration.

Wells	RE II or 6	# analyses	TOC (wt%)	S2 (mg HC / g rock)	Tmax (°C)	HI (mg HC/g TOC)
D001	RE II	3	5.5	26	435	470
D002	RE II	2	4.6	10.6	437	232
D003	RE II	3	4.7	11.5	442	245
D005	RE 6	2	4.2	14.7	436	350
D007	RE II	2	3.9	1.1	439	28
D007	*RE6*	*7*	*2.6*	*0.8*	*456*	31
D012	RE 6	2	5.1	12.6	438	248
D013	RE 6	7	1.9	5.1	443	269
D014	RE 6	7	4.1	17.1	435	418
D015	RE 6	6	2.9	14.3	438	458
D016	RE 6	12	2.5	9.7	439	357
D020	RE 6	19	3.7	20.8	442	562
DZ001	RE 6	111	4.0	12.9	442	319
DZ002	RE 6	183	4.0	11.7	441	288
DZ003	RE 6	55	4.0	19.4	445	482
DZ005	RE 6	26	4.0	10.9	436	267
DZ006	RE 6	38	3.6	8.7	444	237
DZ008	RE 6	17	3.8	16.6	441	435
DZ009	RE 6	22	3.9	13.7	444	346
DZ010	RE 6	25	4.0	15.8	443	394
DZ011	RE 6	13	2.7	8.7	442	323
DZ012	RE 6	35	4.4	11.4	445	261
DZ015	RE 6	35	4.0	10.6	442	260
DZ017	RE 6	34	4.4	12.5	444	280
DZ018	RE 6	40	4.1	10.2	445	251
DZ019	RE 6	35	3.5	6.8	442	195
DZ020	RE 6	30	3.6	6.3	442	175

Table 5. Summary of average TOC values for wells reported in Lavoie et al. (2011), from Anticosti Hydrocarbons L.P. and new D007 (italic) from Junex together with the corresponding average S2, Tmax and HI values. RE II and RE 6 are two different instrument generations for Rock-Eval analyses.

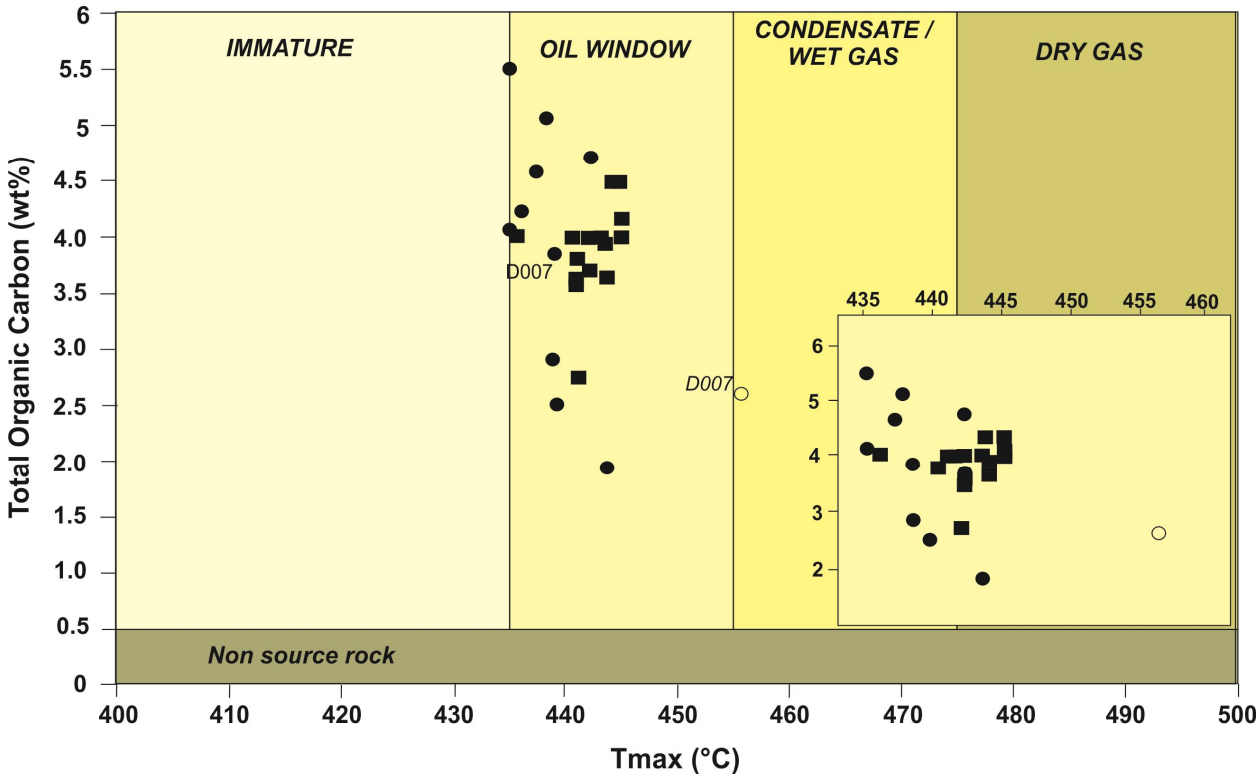

Figure 3. Diagram of Tmax versus Total Organic Carbon. A trend of lower TOC with increasing Tmax value is noted and associated with progressive generation of hydrocarbons. Data in Table 5.In this figure and following ones, filled circles are wells in Lavoie et al. (2011), filled squares are Hydrocarbon Anticosti core holes and open circle is D007 from Junex. The lower right blow-up inset better illustrates the negative correlation between TOC and Tmax.

Figure 4 presents the relationship between the TOC and the S2 value. The relationship is useful to qualify a source rock and its possible origin. At a given TOC value, the content of pyrolisable kerogen is controlled largely by its origin, type and maturity. Type I lacustrine shale have a higher S2 content and are oil-prone compared to a similar TOC content in a Type III terrestrial shale which is largely gas-prone. The distribution of data indicates that all but one well are characterized by Type II/III organic matter, prone to generate oil and gas. The exception being the D007 well, which even if carrying significant TOC, has a very low remaining potential (S2).

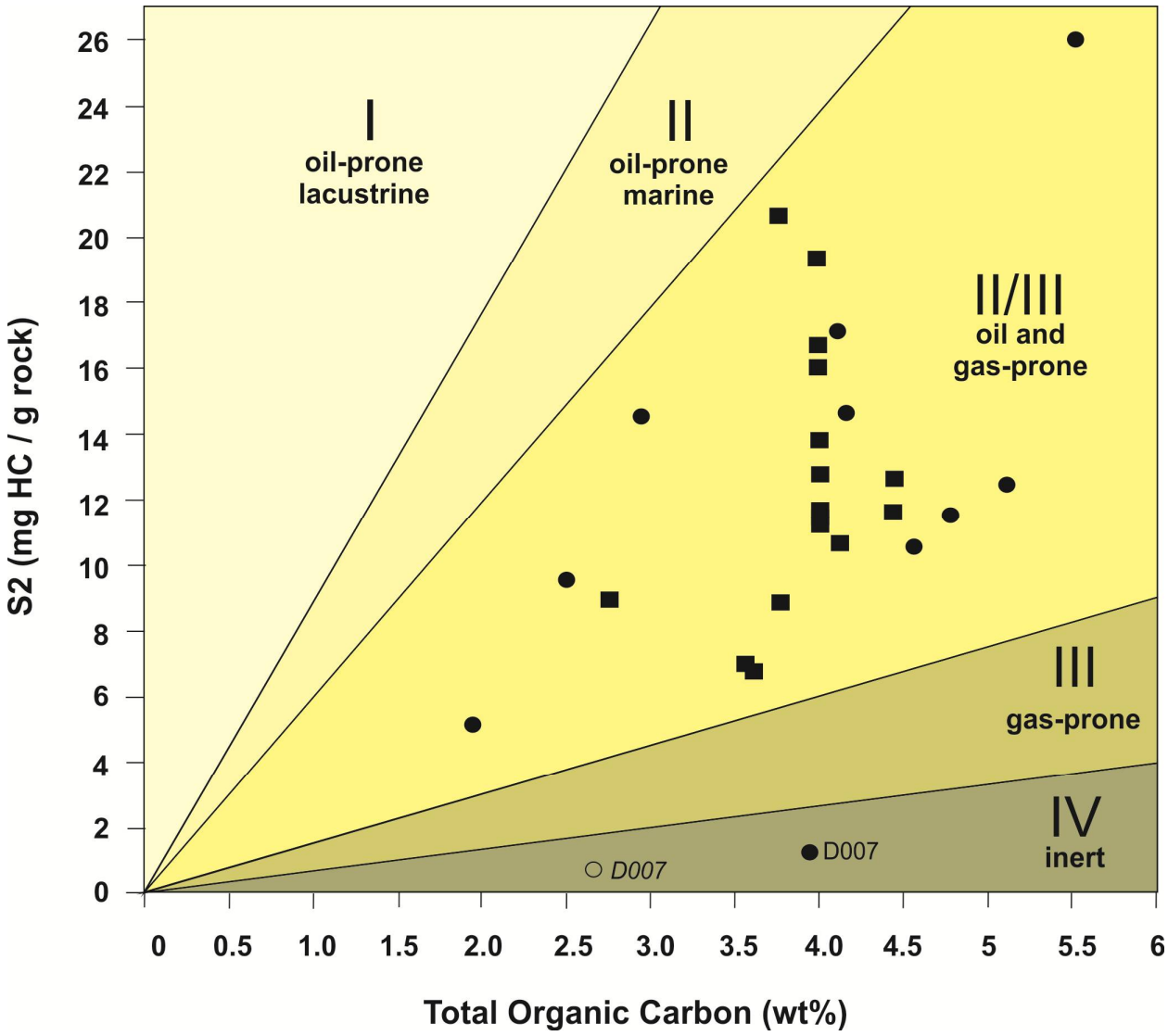

Figure 4. Diagram TOC versus S2. Except for the 2 values for D007, the shales of the Macasty Formation plots in the oil and gas-prone field. Figure 3 for symbols and data in Table 5.

Based on TOC vs S2 diagram, the shales of the Macasty Formation have both oil and gas potential. This potential can be better viewed by reporting on log scale the same information. Figure 5 presents the same TOC vs S2 data with the evaluation of the remaining source rock potential. All wells and core holes, besides D007 plot in the excellent to good potential fields. The Lavoie et al. (2011) and Junex data for the D007 both suggest a poor remaining source rock potential.

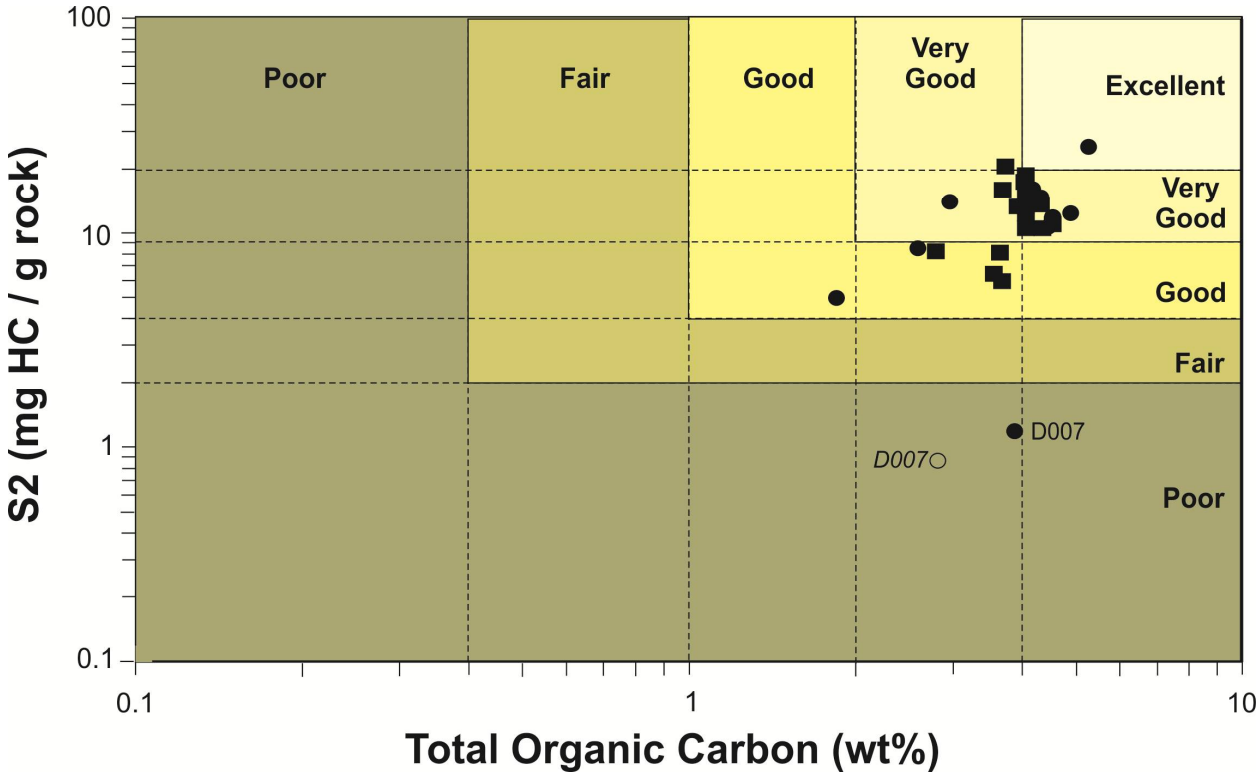

Figure 5. Log-log diagram of TOC versus S2, and qualification of the actual source rock potential of the shales of the Macasty Formation. Figure 3 for symbols legend and data in Table 5.

Figure 6 displays the values of HI versus Tmax and the values of HI versus TOC. The left side of the graphic shows that all wells have organic matter of Type II of marine origin that is in the oil window, with the exception of D007 well. As with other indicators, the wells further to the north and northeast of the island have the highest HI and relatively lower Tmax and conversely, wells south and southwest of the

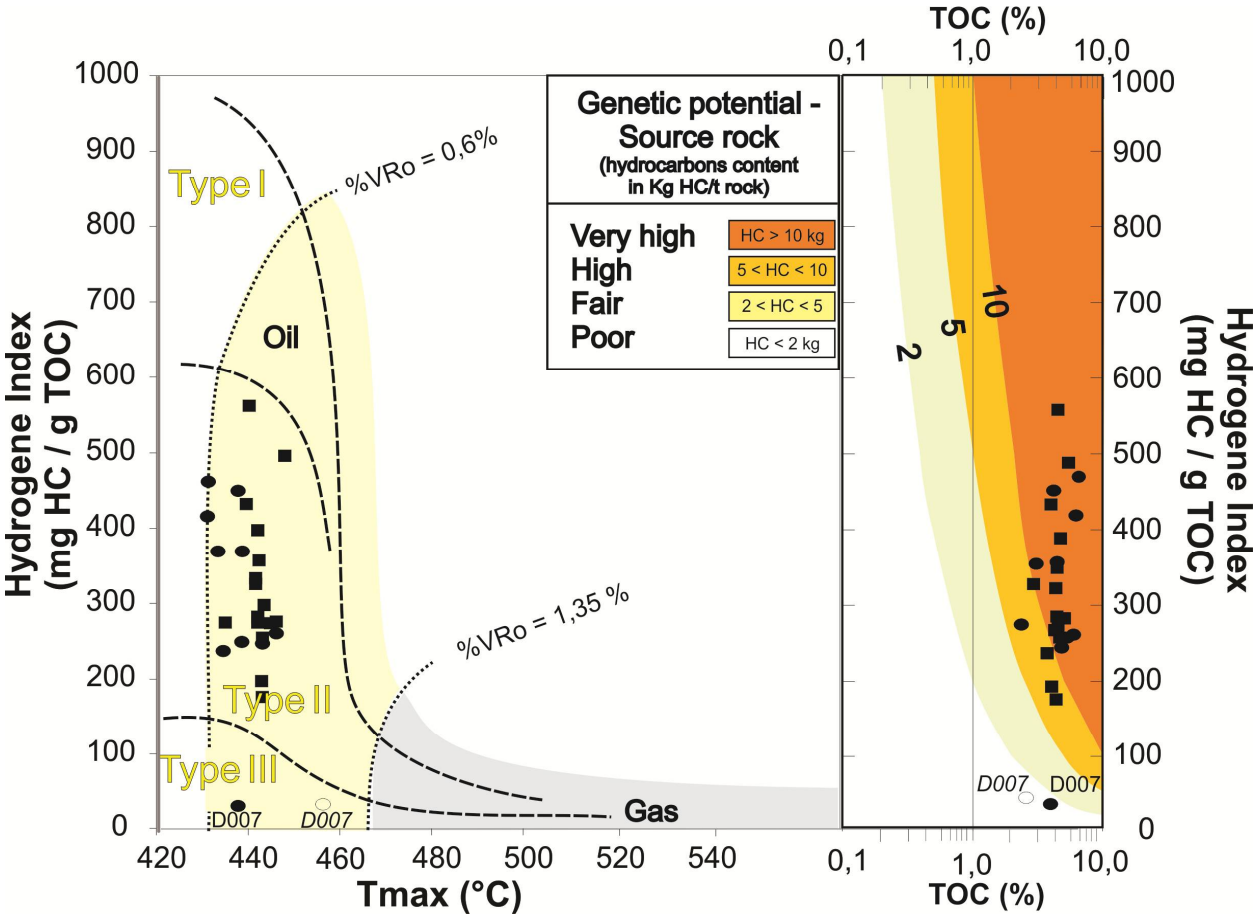

Figure 6. HI vs Tmax and HI vs TOC graphs to illustrate the type of organic matter, its degree of maturation and its current genetic potential. Modified from Espitalié et al. (1977). Data from Table 5.

Jupiter Fault have lower HI. Nonetheless, the data suggest that HI can vary significantly over a narrow range of Tmax. The HI versus TOC plot of the data clearly indicates the high source rock quality and generative potential of the Macasty Formation. The Macasty Formation has a very high potential to generate hydrocarbons.

Type of organic matter

Different types of organic matter will generate different types of hydrocarbons at a given burial temperature, so the understanding of the type of organic matter is a critical element for predicting the nature of the resource to be likely present at a given level of thermal maturation. Bertrand (1987, 1991) petrographically documented the presence of a dominant zooclast population (graptolites, chitinozoans, scolecodonts) with liptinite and bitumen. Such an assemblage is commonly found in Type II marine organic matter. Rock Eval data also allows characterization of the type of organic matter, the best known indicator is the plot of hydrogen index (HI) versus oxygen index (OI) (pseudo van Krevelen diagram).

Figure 7 presents this diagram built with public domain data (Lavoie et al., 2011) on which we have added the average values of HI and OI from the Petrolia 2012 program, the Anticosti Hydrocarbon 12 core holes and new D007 values from Junex. The entire data set plots in the Type I-II marine organic matter.

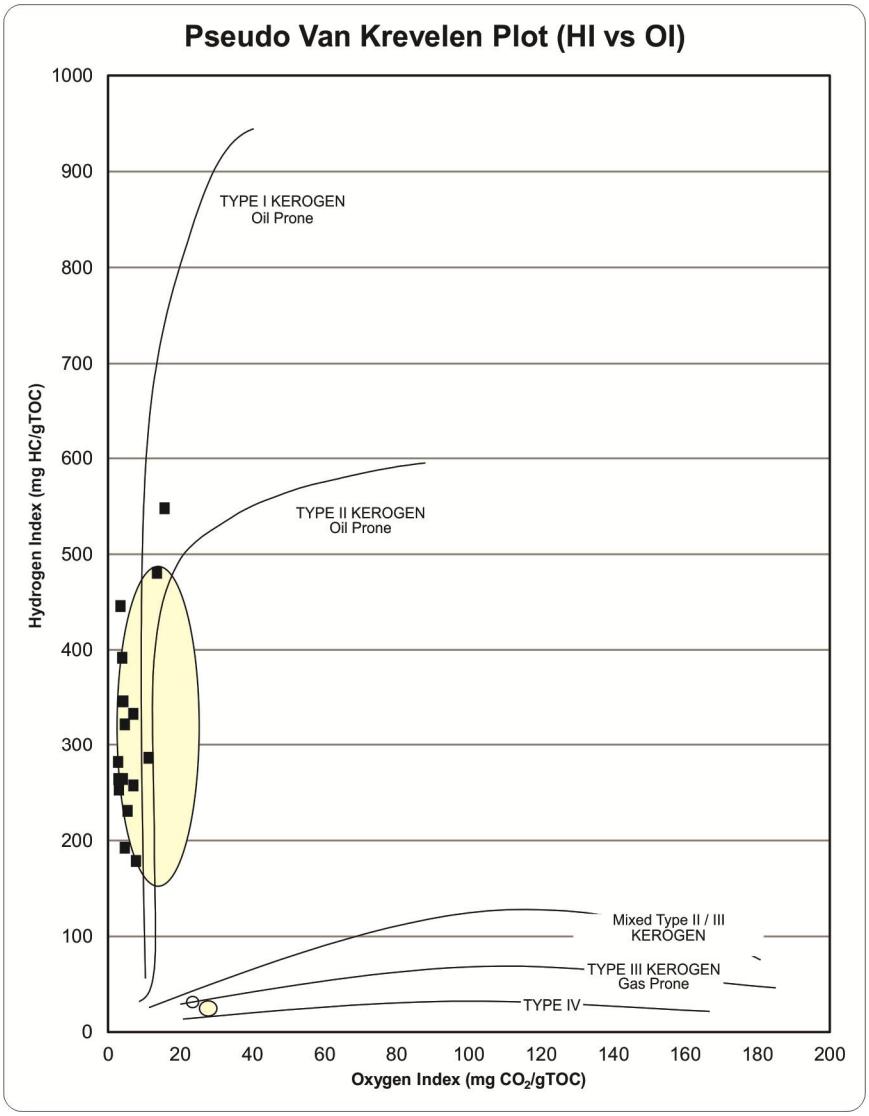

Figure 7. Pseudo van Krevelen diagram for the Macasty Formation based on 10 wells data (yellow envelopes; Lavoie et al., 2011). The hydrogen index (HI) and oxygen index (OI) are indicative of Type II marine organic matter. Added average data for DZ001 to DZ020 and D007. Modified from Lavoie et al. (2011) and supplementary data in Table 3.

Thermal maturation

Various thermal maturation indicators (Tmax, organic matter reflectance and production index) indicate that the Macasty Formation is a thermally mature succession with a southwesterly maturation increase.

History – The first evaluations of thermal maturation for the Anticosti Island succession are those of INRS-Pétrole (1974, 1976) which carried out diverse analyses of thermal indicators that were available at that time (organic matter petrography and reflectance, clay assemblages and illite crystallinity) on D003 and D007 wells. Detailed organic matter reflectance, clay mineralogy and Rock Eval II data for surface outcrops and D001, 002, 003, 007 and 010 wells are detailed in Bertrand (1987) and summarized in Bertrand (1991); the conclusions of which suggest a north-east to south-west increase in maturation of the Macasty Formation from early oil (D001, D010) to dry gas (D007) windows. In the post-2000 conventional exploration era, the operators (Shell, Corridor Resources, Encal, Hydro-Québec Oil & Gas, Petrolia, Junex) focused more on reservoir diagenesis (Lavoie et al., 2005; Lavoie and Chi, 2010) than maturation of the source rock itself, nevertheless, some Rock Eval 6 data were acquired by Shell Canada and partners (D012, 013, 014, 015 and 016; Lavoie et al., 2011). Apatite fission track data were also acquired in order to better constrain the burial and exhumation history (Lynch and Grist, 2002). After 2010, the new phase of exploration was focussed on the unconventional reservoir potential of the Macasty Formation, as such, new data pertinent to the thermal history of the formation have been acquired by the operators on the island, the nature of the hydrocarbon resource (oil, condensate, dry gas) being directly related to the thermal regime.

Tmax –Tmax and other Rock Eval values are routinely used by the industry as a proxy for thermal maturation and genetic potential of a source rock for conventional hydrocarbon systems (Hunt, 1996) as well as for evaluating reservoir quality for unconventional hydrocarbon systems (Jarvie, 2012a). For type II organic matter such as is present in the Macasty Formation, Tmax data set the onset of oil generation at 435°C and condensate and gas window conditions are reached at 455°C (Tissot et al., 1987).

The average of the Lavoie et al. (2011) Tmax data for the Macasty Formation is shown on Figure 8, together with average Tmax values from 3 core holes and Chaloupe D20 well provided by Pétrolia part of their 2012 program, the 12 core holes from Anticosti Hydrocarbon 2014-2015 work program as well as (in italics) Junex average Tmax data for the D007 well. The distribution of Tmax values on the map indicates an increase of Tmax from below 440°C in the north and east sector of the island (D001, D014) to increasingly higher values towards the south and west (440°C < Tmax < 445°C), some exceptions are noted with higher Tmax values (DZ003 core hole) or lower Tmax values (D002) with respect to adjacent wells. A significant discrepancy is noted for the D007 well, with Tmax values of 439°C (early oil window; Lavoie et al., 2011) and of 456°C (condensate; Junex exploration).

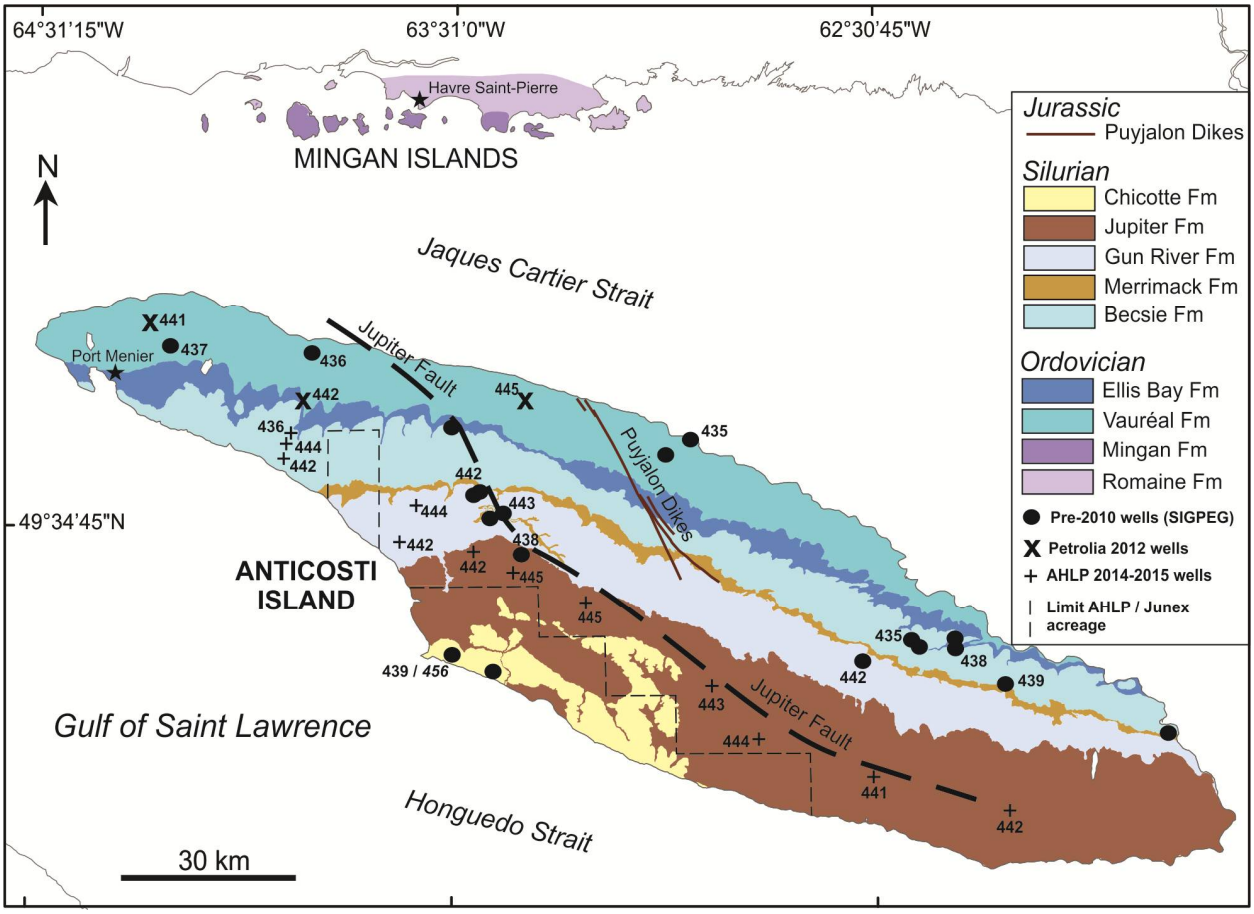

Figure 8. Distribution of average Tmax (°C) values for the Macasty Formation. Data from Anticosti Hydrocarbon L.P. (DZ001 to DZ020 and D20) and Lavoie et al. (2011) for the other wells. Junex D007 well average data is in italic.

Organic matter reflectance – The organic matter components of lower Paleozoic sedimentary rocks differ from younger sediments due to the absence of land plants and terrestrial organic matter and are mainly composed of dispersed organic matter (DOM) of aquatic origin (Hunt, 1996). In the absence of vitrinite, reflectance measurements are carried out on zooclasts (graptolites, chitinozoans, and scolecodonts; Goodarzi and Norford, 1985; Goodarzi, 1985; Bertrand and Héroux, 1987) and solid bitumen (Jacob, 1985; Suárez-Ruiz et al., 2012). The correlation with standard vitrinite Ro is determined through various empirical relations built for specific non-vitrinite kerogen (Hartkopf-Fröder et al., 2015). It is commonly accepted for Type II organic matter that the onset of oil generation is at 0.6%$VRo_{equi.}$, condensates are produced between 0.8 and 1.4%$VRo_{equi.}$ and dry gas dominates at %$VRo_{equi.}$>1.4 (Tissot et al., 1987).

Organic matter reflectance values expressed as %$VRo_{equi.}$ are shown on Figure 9, the data was provided by Anticosti Hydrocarbons, June provided the organic matter reflectance data they generated for the D007 well (shown in italic). A similar map pattern compared to Tmax is observed with the lowest

%VRo$_{equi.}$values (0.76 to 0.86%; oil window to early rich condensate zones) in the north and eastern part of the island and significant increase towards the west, on the downthrown block of the Jupiter Fault, to values ranging between 0.9 and 1.85% (lean condensate to dry gas). A significant difference in %VRo$_{equi.}$ data for the D007 well is noted between Anticosti Hydrocarbons (1.85%; dry gas) and Junex (0.9%; rich condensate zone).

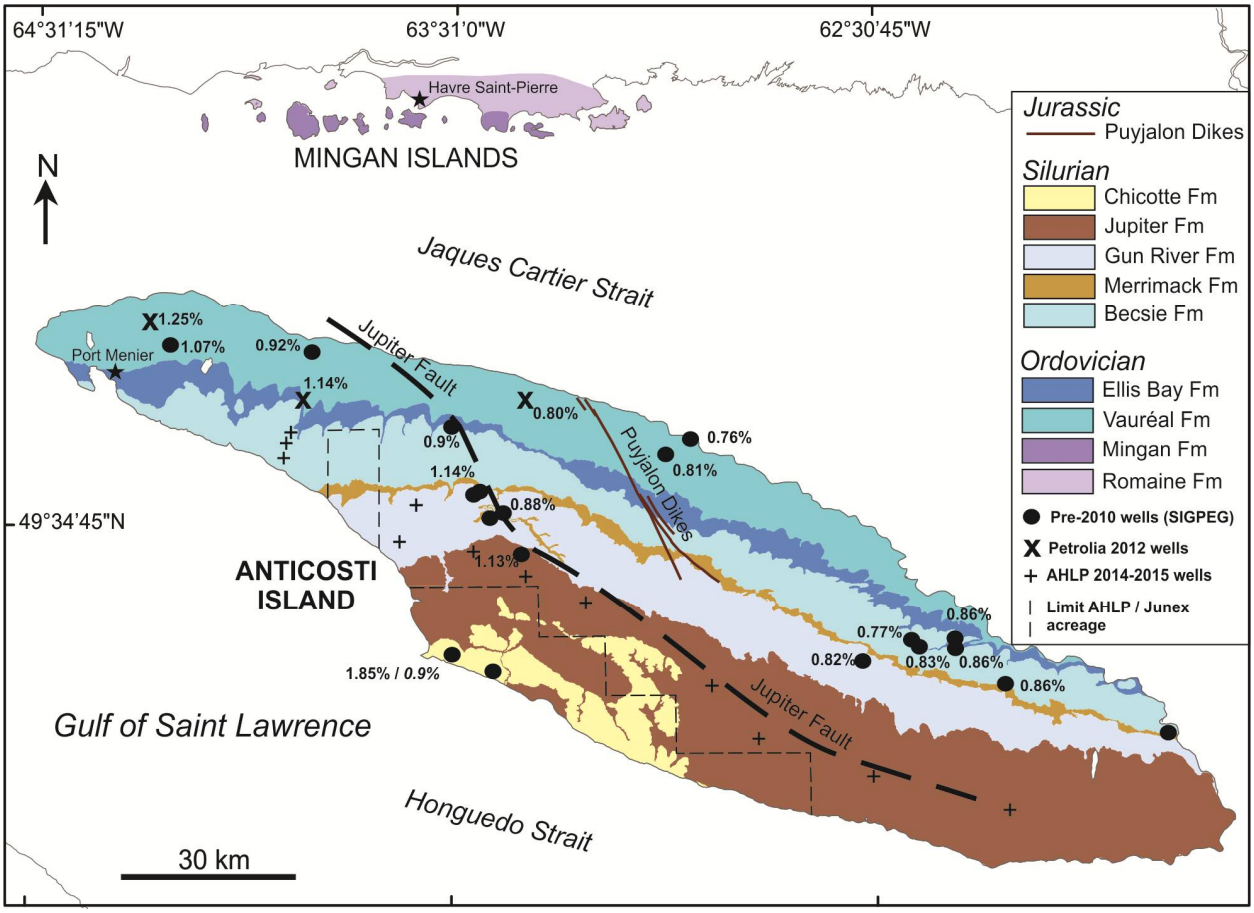

Figure 9. Distribution of average %VRo$_{equi}$ for the Macasty Formation. Data from Anticosti Hydrocarbons and Junex (in italic, D007 well).

Production index (PI) or transformation ratio – The production index (PI) is another Rock Eval-derived indicator of thermal maturation. PI is the result of the S1 value divided by S1+S2, therefore it relates the volume of free volatiles (S1) in the rock with respect to the total hydrocarbons (produced or S1 and remaining potential or S2). An immature rock will have a PI of 0, hydrocarbons only start to be generated at a PI of 0.1 and an overmature rock will have a PI of 1. The PI is commonly graphically represented with its related Tmax and / or %VRo$_{equi}$ values which can help to distinguish charge events (excess S1 at given Tmax or %VRo$_{equi}$).

Table 6 presents the PI values for the wells found in Lavoie et al. (2011), the 3 core holes and Chaloupe (D20) well from Petrolia, the 12 core holes from Hydrocarbon Anticosti and the new data for D007 well from Junex. Together with the PI, the number of analyses, the type of Rock Eval machine (old RE II or recent RE 6), the Tmax and $\%VRo_{equi}$ values are provided. The PI averages are plotted on the Anticosti map (Fig. 10). A pattern similar to those noted from Tmax and $\%VRo_{equi}$ is noted, wells located north and east of the Jupiter Fault have low PI values ($0.1<PI<0.16$), slightly above 0.1 indicating onset of oil generation. These PI values slightly increase towards the fault (D020). Southwest of the Jupiter Fault, PI values increase from 0.14 (D005) to 0.58 (D007), suggesting increased oil generation from kerogen due to an increase in paleo-burial depths south of the fault. The PI data is plotted against Tmax values (Fig. 11) and $\%VRo_{equi}$ (Fig. 12) to evaluate the degree of kerogen transformation into hydrocarbons.

Wells	RE II or 6	# analyses	P1 S1/(S1+S2)	Tmax (°C)	$\%VRo_{equi}$
D001	RE II	3	0.12	435	0.76
D002	RE II	2	0.37	437	1.07
D003	RE II	3	0.14	442	1.14
D005	RE 6	2	0.14	436	0.92
D007	RE II	2	0.58	439	1.85
D007	*RE6*	*7*	*0.58*	*456*	*0.9*
D012	RE 6	2	0.22	438	1.13
D013	RE 6	7	0.13	443	0.88
D014	RE 6	7	0.10	435	0.77
D015	RE 6	6	0.10	438	0.86
D016	RE 6	12	0.13	439	0.86
D020	RE 6	19	0.16	442	0.82
DZ001	RE 6	111	0.20	442	1.14
DZ002	RE 6	183	0.29	441	1.25
DZ003	RE 6	55	0.10	445	0.8
DZ005	RE 6	26	0.26	436	N/A
DZ006	RE 6	38	0.24	444	N/A
DZ008	RE 6	17	0.15	441	N/A
DZ009	RE 6	22	0.13	444	N/A
DZ010	RE 6	25	0.16	443	N/A
DZ011	RE 6	13	0.19	442	N/A
DZ012	RE 6	35	0.20	445	N/A
DZ015	RE 6	35	0.25	442	N/A
DZ017	RE 6	34	0.19	444	N/A
DZ018	RE 6	40	0.19	445	N/A
DZ019	RE 6	35	0.27	442	N/A
DZ020	RE 6	30	0.27	442	N/A

Table 6. Summary of PI values for wells reported in Lavoie et al. (2011), from Anticosti Hydrocarbons L.P. and new data for D007 (Junex, in italic) together with Tmax and $\%VRo_{equi}$. PI is for Production Index. RE II and RE 6 are two different instrument generations for Rock-Eval analyses.

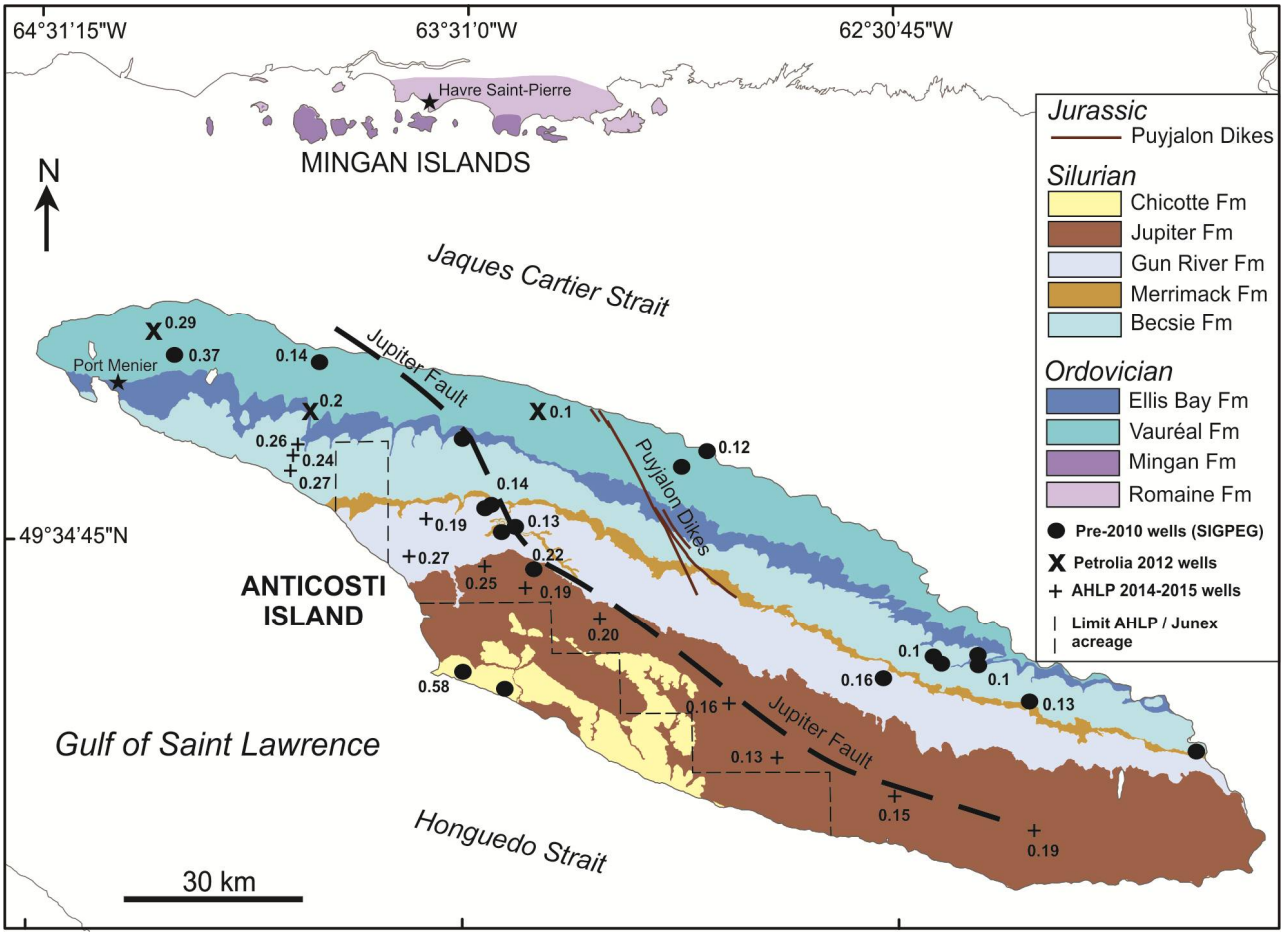

Figure 10. Distribution of average PI values for the Macasty Formation. Data in Table 6.

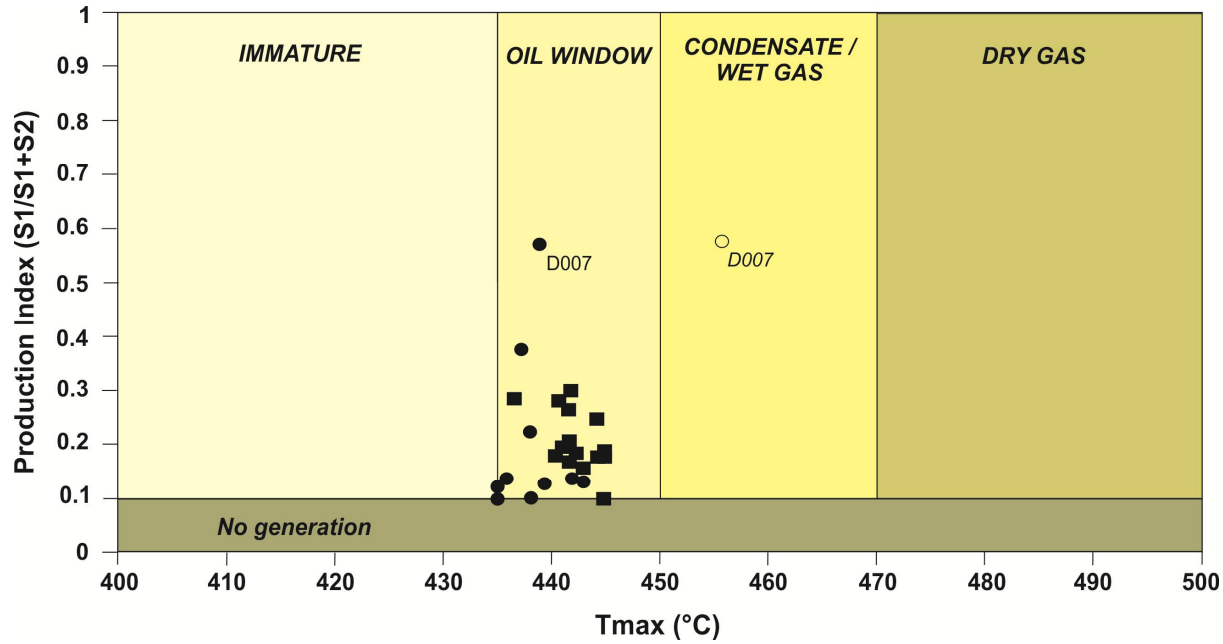

Figure 11. Diagram PI versus Tmax. Figure 3 for symbols legend and data in table 6.

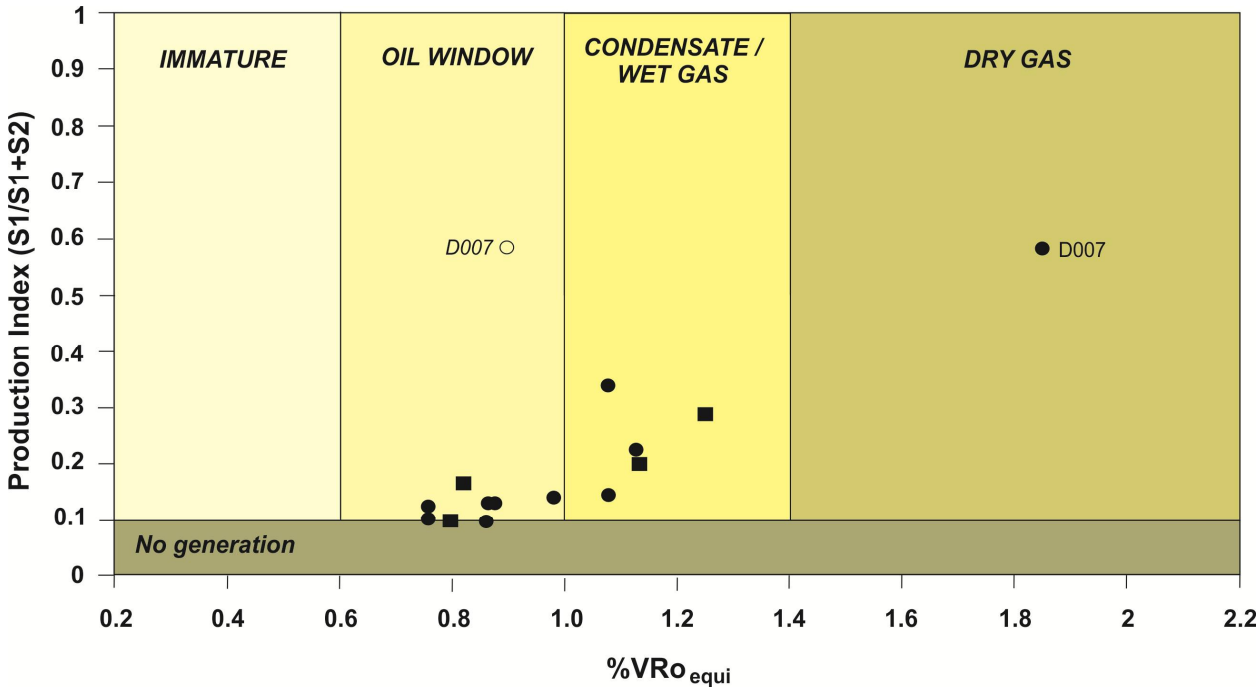

Figure 12. Diagram PI vs $\%VRo_{equi}$. Figure 3 for symbols legend and data in Table 6.

It is noteworthy that there is a general consistency between PI and Tmax / $\%VRo_{equi}$ as in both cases the wells with higher PI also have higher Tmax and $\%VRo_{equi}$. However, the average $\%VRo_{equi}$ values seem to indicate higher maturation level than the Tmax values do. On Figure 11, no average Tmax values suggest condensate zone, even for wells south of the Jupiter Fault; whereas all wells southwest of the Jupiter Fault have PI vs $\%VRo_{equi}$ plots suggestive of the condensate / wet gas window (Fig. 12).

Discussion on thermal indicators – The available dataset of thermal indicators is consistent for both Tmax and $\%VRo_{equi}$, the area northeast of the Jupiter Fault is less mature compare to the area southwest of that fault (Figs. 7 to 9). From current Tmax dataset, the area near the northwest end of the island is the most mature, whereas based on $\%VRo_{equi}$, it is the area near D007 that is the most mature.

The available data set for the D007 well is worth further discussion. Tmax values reported in Lavoie et al. (2011; 439°C) are about 17°C lower than that reported by Junex (456°C). However, the PI values from Lavoie et al. (2011) and Junex Exploration are comparable, both at 0.58 suggestive of significant transformation of kerogen to hydrocarbons. In addition, they also reported similar HI values (*ca* 28 vs 31 mg HC/g TOC) for samples analyzed from the D007 well. Considering the high HI values (e.g. 300 to 500; mg HC/g TOC; Figure 7) displayed by all other marginally mature Macasty shale samples, the Macasty shales at the D007 well seem to be at an advanced stage of kerogen transformation, and their Tmax values are most likely around 450 - 460°C, placing the shale interval at the limit between the oil and condensate windows.

The problem with the Tmax reported by Lavoie et al. (2011) may be related to the exact stratigraphic assignment of the samples submitted for Rock-Eval analysis. The reported depths (2392 m and between 2398 – 2487 m; for Lavoie et al. (2011) and Junex, respectively) are correlative with the Macasty Formation, it is possible, but yet speculative, that cuttings analysed might have been contaminated from cavings, although HI values for units overlying the Macasty in the D007 well are all above 100 mg HC/ g TOC (Bertrand, 1987).

Rock Eval pyrograms are commonly evaluated to ascertain the degree of precision of the Tmax (maximum temperature of the S2 peak), samples with low HI commonly have relatively flat S2 curve making the exact determination of the S2 peak a challenge. Unfortunately, the pyrograms for the Macasty Formation samples are not available.

Chi et al. (2010) based on numerical modeling, have suggested that significant overpressure regimes developed in the Vauréal – Macasty formations due to rapid sediment accumulation, compaction and hydrocarbon generation at maximum burial time. The maximum of overpressure occurred in the area south of the Jupiter Fault. Numerous studies have proposed that overpressure will retard the maturation of organic matter and hence will result in lower and erratic thermal estimates for both $\%VRo_{equi}$, (Carr, 1999; Zou and Peng, 2001; Chatellier et al., 2013) and Tmax (Chatellier et al., 2013). In the D007 well report, it is noted that the mud weight had to be significantly increased in the lower part of the Vauréal Formation indicating an increase in pressure. However, the effects of overpressure on $\%VRo_{equi}$, reported in Bertrand (1991) and from Anticosti Hydrocarbons (2.07 and 1.85%, respectively) are not detected.

Finally, it is also possible, but still speculative, that the lower HI values might be related to the fact that the Macasty Formation is experiencing a facies transition towards the south-west as it gets closer to the Taconian foreland (Pinet et al., 2012).

Therefore, the exact cause(s) for the strong divergences between dataset for the D007 well is/are still unknown. However, the new Tmax values of Junex Exploration (456°C, Table 4) are more in line with the regional distribution of other Tmax values with a southwest increase of data.

PETROLEUM RESOURCE ASSESSMENT

Methodology

The method used in this petroleum resource assessment is a volumetric approach with a dual-porosity model that quantifies the reservoir storage for oil and gas. The dual porosity model is designed for evaluating resource potentials in a shale play, in which both the matrix and organic porosities are effective storage for oil and gas accumulations. The dual porosity model assumes that there are two major porosity systems (Fig. 13a and b) that are controlled by different geological processes in a shale source rock reservoir. The matrix porosity decreases with burial depth as a result of mechanical compaction and

diagenesis (Fig. 14). Studies suggest that mineral composition, grain size, texture of the sedimentary rock, compaction and diagenetic history are primary factors affecting matrix porosity (Dutton and Loucks, 2010; Ramm, 1991). Matrix porosity shows a remarkable change at a depth around 2500 metres, above which the decreasing rate in porosity is rapid and the primary control is mechanical compaction. Below 2500 metres, the decreasing rate becomes slower and chemical (diagenesis) compaction plays a more important role.

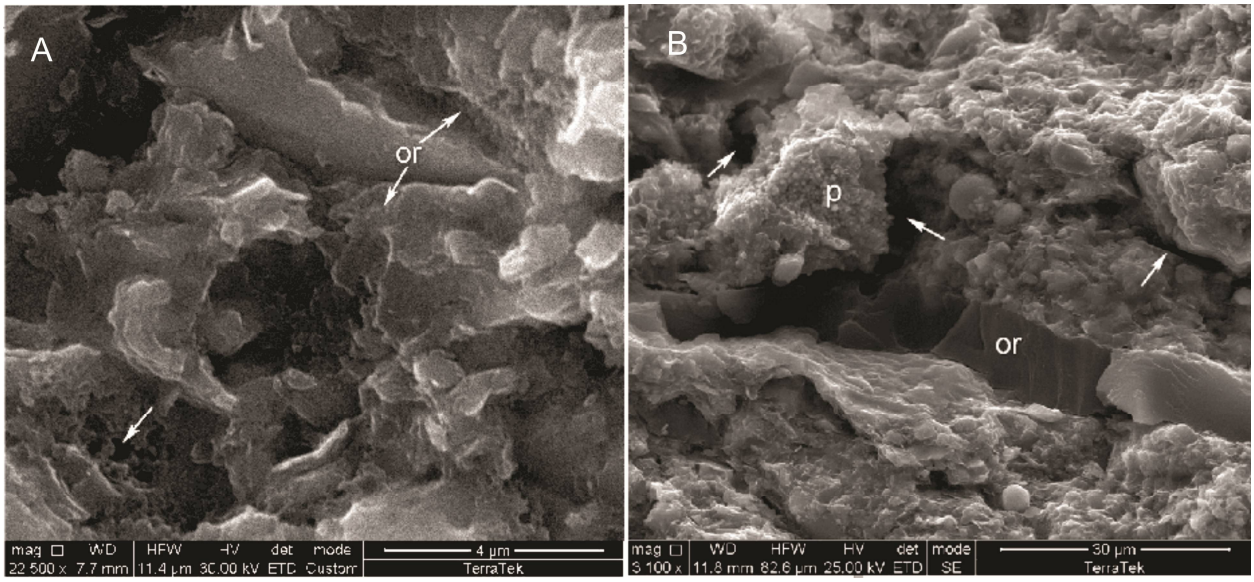

Figure 13: Scanning electron microscopic (SEM) images of core samples of the Macasty Formation in DZ001 well showing two different types of pore systems developed in the source rock reservoir. A: SEM image of nanometer-scale pores (arrow) associated with organic matter (or). These pores contribute to the effective porosity and pressure-decay permeability measurements of 5.34% of BV and 205 nD, respectively. [Scale Bar = 4 microns, Depth: 1147.0 m]. B: SEM image showing large interparticle pores (arrows) occur between crystals/grains and the surrounding matrix. Organic matter (or) in particle form is aligned with clay laminations and sits adjacent to diagenetic pyrite (p). [Scale Bar = 30 microns. Depth: 1137.0 m].

In contrast, organic porosity increases with thermal maturity in the hydrocarbon generation windows. The abundance and size of organic pores are a function of thermal maturity, richness and type of organic matter. The organic porosity originates from conversion of organic matter (kerogen) to oil and gas. No significant organic porosity is formed above the oil generation window and organic porosity approaches the maximum at the end of oil generation window. This is supported by theoretical calculation of mass balance and visual evidence from scanning electron microscopic (SEM) images of various thermal maturities (e.g., Chen and Jiang, 2016). Figure 13a shows example organic pores within organic matter from SEM image of core sample of Macasty Formation. Organic porosity may decrease from the end of oil generation window as a result of pyro-bitumen precipitation due to thermal cracking of oil to gas (Pepper and Dodd, 1995).

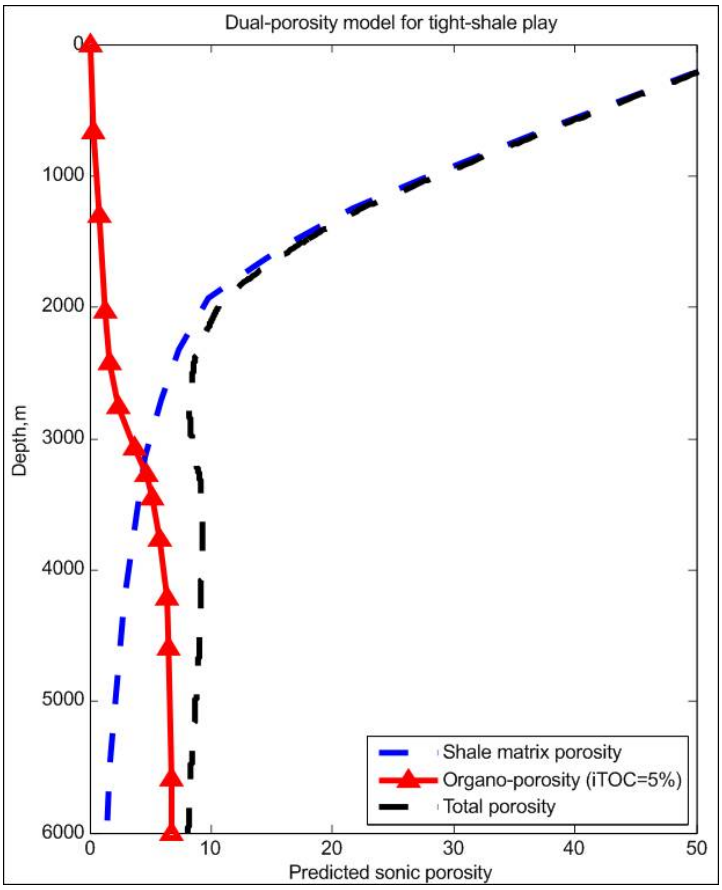

Figure 14: Schematic diagram showing general characteristics of two different porosity trends in a shale basin (lithic matrix micro-porosity and organic nano-porosity). The matrix porosity decreases with depth; whereas the organic porosity increases with depth. These two porous systems are results of different geological processes and have distinct physical and chemical properties in terms of storage of oil and gas. iTOC in the diagram indicates initial TOC.

Hydrocarbons retained in source rocks are stored in both matrix and organic pores. Differentiating these two porosity systems is necessary because of the unique characteristics of each pore type for hosting hydrocarbons. A matrix pore is likely to be water wet with layers of bound water. The size of pore is at micrometre scale and no significant adsorption gas exists. In contrast, an organic pore is likely oil-wet and there is no water layer in the pore. The pore size is at nanometer scale, close to the hydrocarbon molecular size (<1 nm for methane up to 40 nm for asphaltines; Momper, 1978), thus contain a large amount of adsorbed gas. Figure 15 presents a schematic model of the dual porosity system, demonstrating the key characteristics and differences of the two porosity systems.

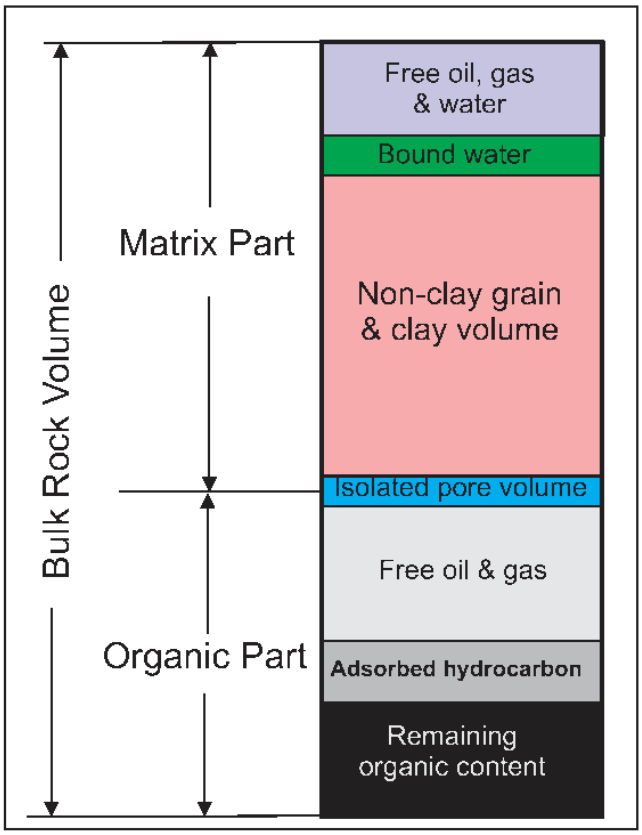

Figure 15: A schematic model for resource estimation in a shale play where both matrix porosity and organic porosity contribute to the storage of oil and gas accumulation (modified from Ambrose et al. 2012). The percentage of the various components forming the bulk of the rock volume is schematic and does not intent to represent a specific case.

The hydrocarbon volumes in the two different porosity systems are estimated from geochemistry data and geophysical well logs separately. Additional laboratory test is necessary to determine the capacity for adsorbed hydrocarbon. Figure 16 is a workflow chart showing the processes and components for the estimation of hydrocarbon pore-volume under the dual-porosity model. The mathematical formulations of the volumetric calculation of different hydrocarbon components and application examples were presented in Chen et al. (2014) and are not described in this document. In this study, we treat the volumetric variables, such as hydrocarbon saturated porosity, reservoir net thickness and hydrocarbon pore volume as spatial random variables. The spatial variations of these parameters and their uncertainty were evaluated through contour interpolation (kriging), a spatial statistical method for data interpolation which gives the best linear and unbiased prediction of intermediate data (Journel, 2013).

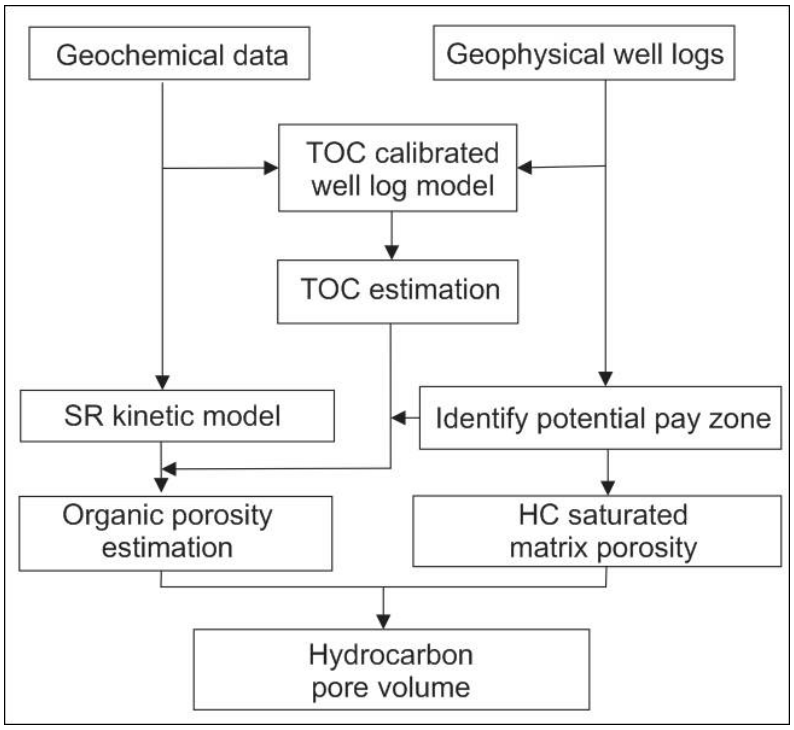

Figure 16: A flow chart demonstrating the work flow and components for hydrocarbon pore volume estimation using geochemical and well log data under the dual-porosity model.

The total percentage of hydrocarbon saturated porosity multiplied by the total net rock volume (Fig. 2) will provide the hydrocarbon pore volumes (Fig. 16). The total net volume of the Macasty Formation was calculated from thickness data and surface area covered by the unit, data are presented in Table 1 and from a modified 3D geological model for Anticosti island (Bédard et al., 2014).

Thermal Maturity and Hydrocarbon Generation Models

Two thermal maturity indicators are available for thermal maturity model construction: Tmax from Rock-Eval pyrolysis and vitrinite reflectance equivalent (%VRo_{equi}) from organic matter reflectance measurements. As large discrepancies exist in available %VRo_{equi} data (Figure 17a and previous sections), a one dimensional (1D) thermal history and maturity model of the Arco Anticosti #1 well (D007) was constructed. The burial history model for the D007 well is adapted from a hydrocarbon migration modeling study of the Anticosti Basin (Chi et al., 2010). The predicted %VRo_{equi} follows a trend that is lower than the Anticosti Hydrocarbons dataset and higher than the Junex dataset (Fig. 17a). The predicted %VRo_{equi} at the base of Macasty Formation (2487 m) is about 1.6%, suggesting a thermal maturity close to the end of the hydrocarbon generation window.

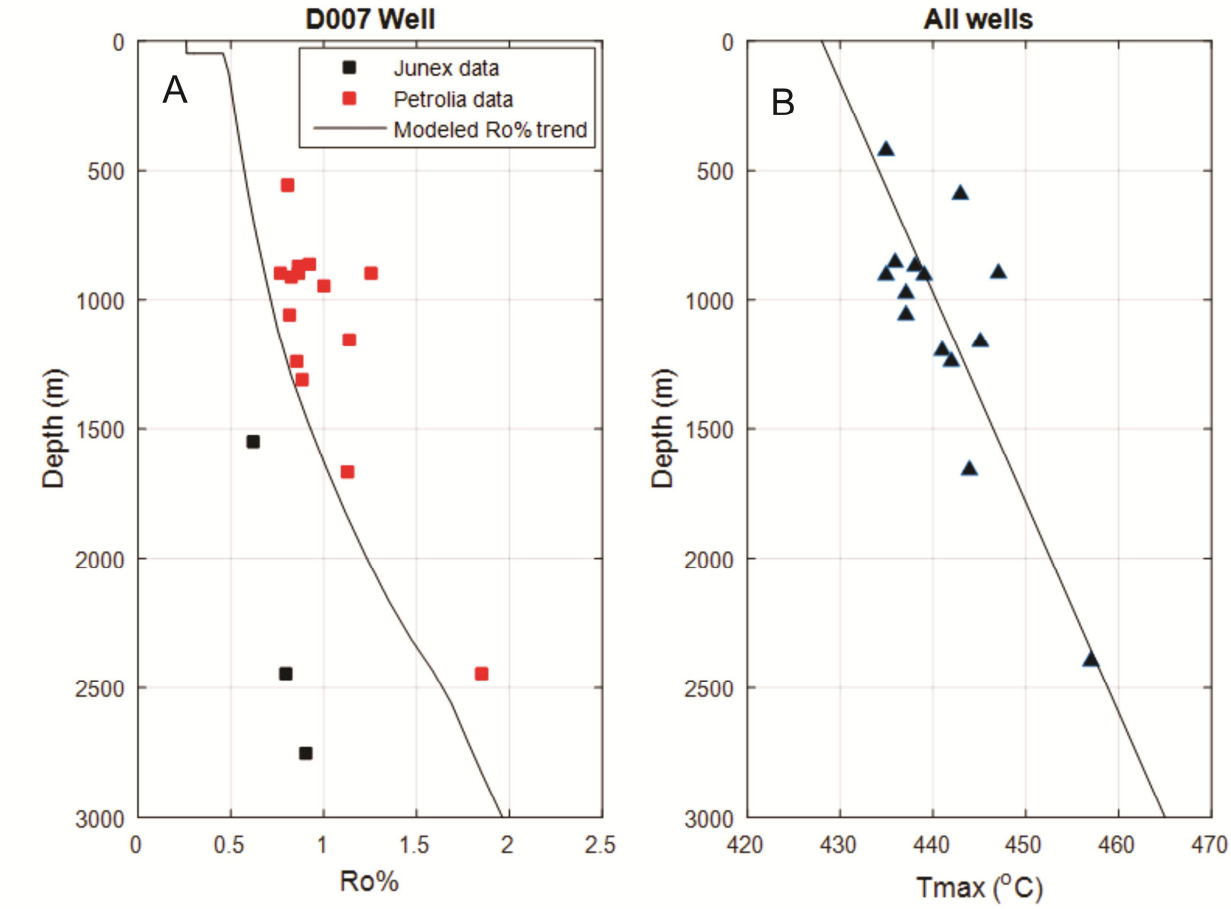

Figure 17: Left: comparison of observed $\%VRo_{equi}$ data and thermal maturity model from 1D thermal history modeling. Right: average Tmax in each well versus depth showing the general trend of Tmax increasing with depth of the Macasty top.

The maturity and hydrocarbon generation models were constructed using Tmax data because of data discrepancies in vitrinite reflectance equivalent measurements from different sources (Figure 17). In addition, Tmax can be used jointly with other bulk rock geochemical properties such as hydrogen index (HI) to provide supplementary information with respect to hydrocarbon generation kinetics, which is critical for hydrocarbon generation modeling (Chen and Jiang, 2015). The hydrogen index and Tmax data are plotted (Figure 18a) to represent the thermal decomposition trajectory of organic matter (hydrocarbon generation) with increasing temperature. Figure 18a shows the data and the decreasing trend of remaining generation potential with increasing thermal maturity. A model is fitted to the data to represent the generalized trend of kerogen decomposition and is then converted to hydrocarbon transformation ratio, representing the degree of conversion of active organic carbon in the kerogen to hydrocarbon (Figure 18b).

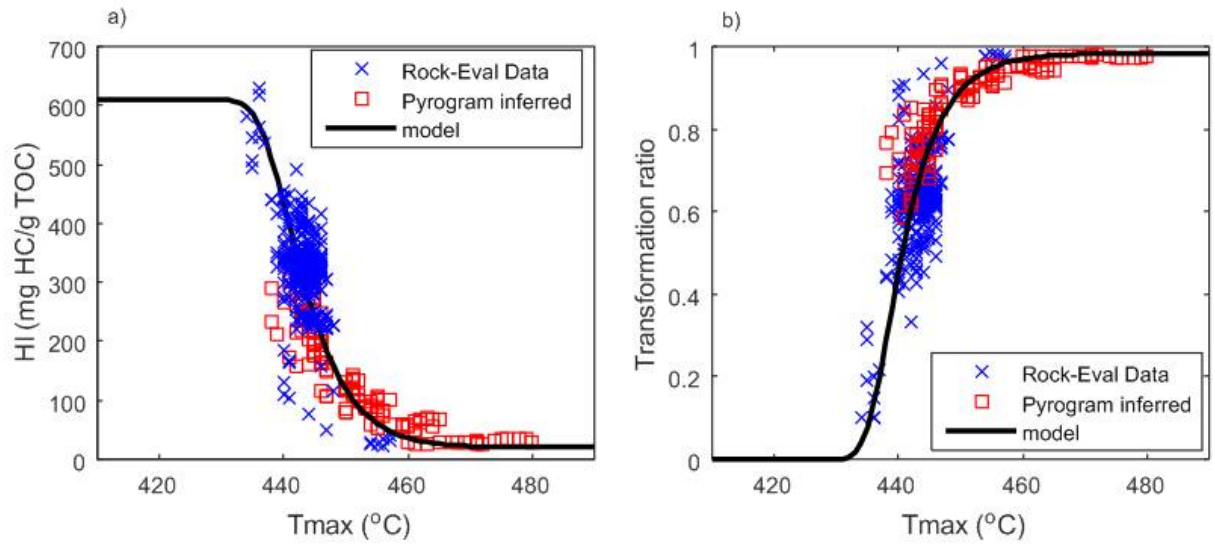

Figure 18: Hydrocarbon generation model constructed from Rock-Eval data. Kerogen decomposition is indicated by the trajectory path of decreasing hydrogen index with increasing Tmax (a). Hydrocarbon transformation ratio (TR) is calculated from hydrogen index (b) using an empirical relationship between HI and TR in Chen and Jiang (2015).

These thermal maturity and hydrocarbon generation models are validated using different data, including direct and indirect evidence. For example, numerically inversed kerogen thermal decay paths are plotted (red rectangles in Figs. 18a and b) along with the data and fitted models to support the generalized trend of the hydrocarbon generation as a comparison. The model can also be validated by Rock-Eval data in D007 well. Given a type II kerogen of initial hydrogen index close to 600 mg HC/g TOC (Fig. 18a), an average hydrogen index of 32 mg HC/g TOC from eleven core samples suggest a transformation ratio of >95%, which is consistent with the transformation model in Figure 18b.

Figures 19a and b are ratios of S1/TOCx100 and S2/TOCx100 (HI) against depth showing the approximate depth ranges for peak oil generation, and oil and gas generation windows. The evolution, with depth, of S1/TOCx100 defined as the Bitumen Equivalent Index (BEI) (Espitalié et al. 1987) shows a general trend of the retaining hydrocarbon (most likely in liquid phase) in the samples and indicates the most likely depth range for occurrence of liquid hydrocarbon. The area present inside the data envelope (broken dashed line) between the upper and lower intercepts with the BEI of 100 represents the oil generation window, the domain with IEB lower than 100 (left) in shallow depth (<500 m) is characterized by a lower transformation ratio compared to the domain with IEB higher than 100 (right).

The S2/TOCx100 (HI) with depth depicts a general decreasing trend of hydrocarbon generation potential with depth, a similar trend indicated by Tmax in Figure 18a. Statistics showed that samples with S1/TOC >1 in wells from producing basins in the US are coincident with oil production zones and is also an indication of oil generation window in source rock reservoir (Jarvie, 2012a). The oil generation

window defined by S1/TOCx100 > 100 shown in Figure 19a spans from 500 to 2000 metres in present day depth corresponding to 0.6% to 1.2% VRo_{equi} data and Tmax range of 433 to 452°C (Figs. 17a and b). Chi et al. (2003) suggested a total of 1400 metres of erosion post exhumation at the D007 well area after the maximum burial at around 280 million years ago. This erosion estimate gives a paleo-depth range of oil generation from 2000 to 3500 metres at maximum burial. The interpreted oil generation window represented by Si/TOCx100>100 is also supported by petrological evidence. Scanning electron microscopy images of core samples in the DZ001 well (Figure 13a) show various nano-pores from a few tens to around hundreds of nanometre within the organic matter in the Macasty Formation (depth range from 1133 to 1188 metres), indicating that considerable amount of organic matter has been converted to hydrocarbon (oil and gas) generating various void space within the organic matter; this provides direct evidence that the source rock has entered major hydrocarbon generation window at that depth range. Other direct evidence of oil generation windows is the fact that the Macasty core from the Pétrolia/Corridor Chaloupe well contained residual oil (Carsted, 2011).

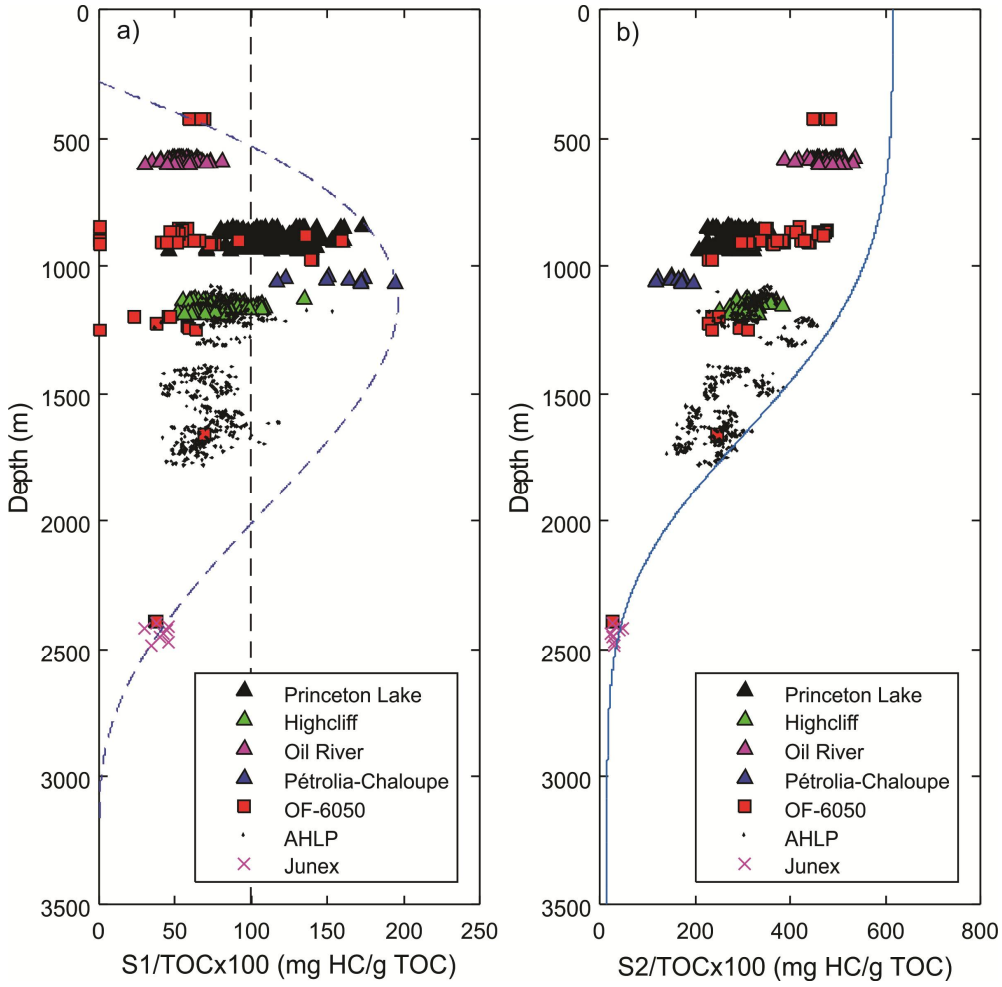

Figure 19. Depth profiles of S1/TOCx100 (A) and S2/TOCx100 (B) with depth showing the general trends of retained hydrocarbons (S1) and hydrocarbon generation potential (S2) with depth in the Macasty

Below 2000 metres (%VRo_{equi} > 1.2%), the Macasty Formation enters the gas generation window Fig. 19a) and natural gas becomes dominant because of thermal cracking of oil to natural gas at higher temperatures. The maturity range for gas generation is comparable with other unconventional shale oil play, such as the Eagle Ford and Barnett shale oil zones (Jarvie, 2012a; Cander, 2013). The presence of natural gas is also supported by petrophysical data such as evidenced by density and neutron porosity cross over and lowered sonic velocity in D007 wells at a depth range of 2405-2487 metres (Fig. 20). Other indirect evidence, such as mass-balance calculation and well log anomalies also supports the thermal maturity and hydrocarbon generation models and will be discussed in the following section.

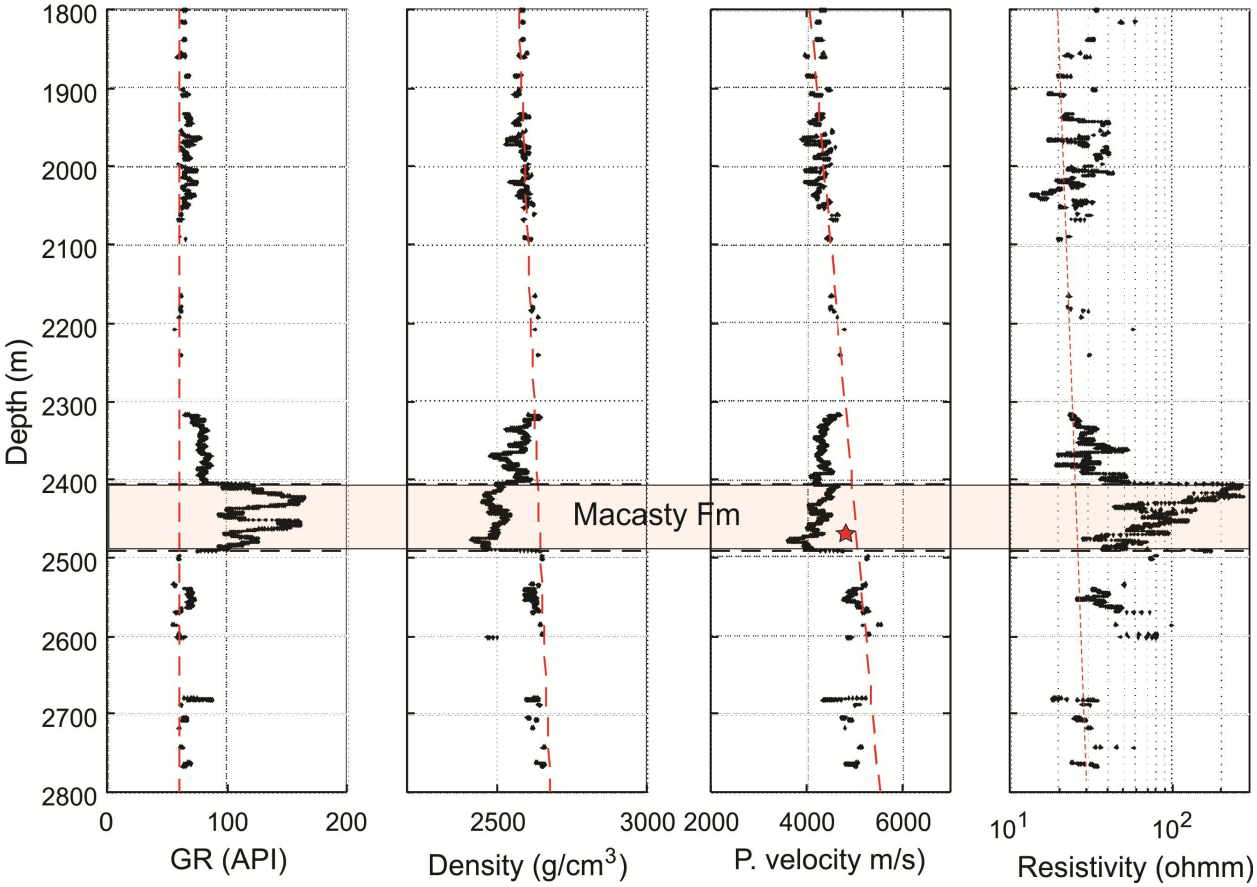

Figure 20. Well log responses to shale intervals in D007 well. Well log data points are selected by criteria of GR>65 API and no obviously enlarged borehole condition to remove impacts from lithology and borehole environmental conditions on the well log responses. The Macasty Formation in D007 well shows a high GR (1st column), low p-wave velocity (2nd column) and density (3rd column), and high resistivity (4th column). The star denotes the abrupt decrease on the p-wave velocity log at the base of the Macasty Formation.

Volumetric Parameter Estimation

Data analysis suggests that TOC is proportional to laboratory measured porosities (effective and hydrocarbon saturated) (Fig. 21), suggesting that organic pores are a major contributor to hydrocarbon saturated porosity. It is interesting to note that a) the higher the maturity (e.g. Princeton Lake), the steeper the slope is (higher porosity for samples with the same amount of initial TOC); and b) the linear relationship from each well on Figure 21a terminates at ~1.5% hydrocarbon saturated porosity base line, which may indicate the contribution from matrix porosity is around 1.5%. The co-existence of matrix and organic porosities, and their relative abundance in the Macasty Formation is supported by the microscopic images (Fig. 13).

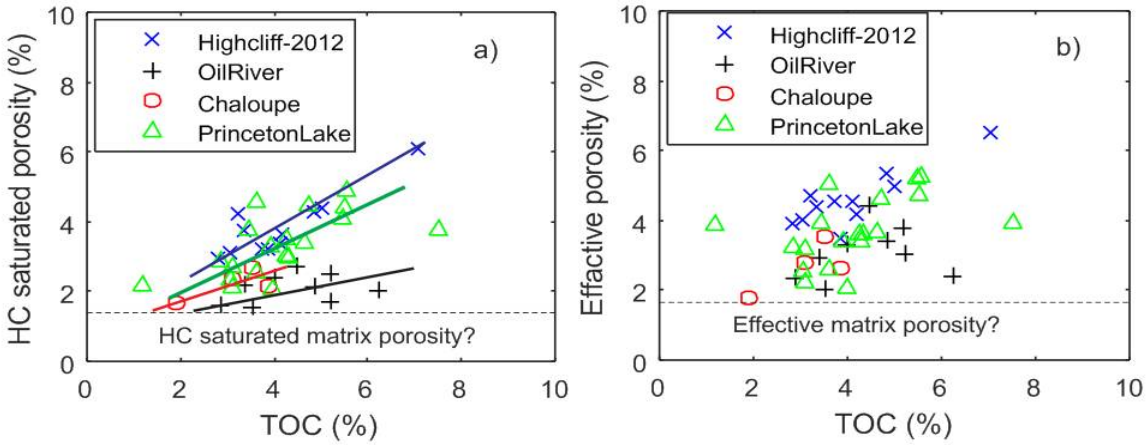

Figure 21. Relationships between TOC and different porosities. a) TOC with HC saturated porosity. On this diagram, higher thermal maturation correlates with a steeper correlation slope; b) TOC with effective porosity.

Organic porosity estimation

Organic porosity is calculated using the revised mass balance method by Chen and Jiang (2016). The organic porosity, $\emptyset_{org}$, can be estimated by converting the amount of carbon transformed to hydrocarbon from a weight percentage to a volume percentage, which is expressed in the following form:

$$\emptyset_{org} = \gamma[C_{toc}^{o}\alpha T_R\left(1-\frac{0.833C_{toc}}{100}\right)]\frac{\rho_b}{\rho_k} \qquad (1)$$

where C_{toc}^{o} is the initial TOC content (w%), T_R, the transformation ratio (fraction), $\rho_b and\ \rho_k$ are bulk rock density and the density of kerogen respectively; and γ represents the carbon equivalent mass of kerogen in hydrocarbon conversion (γ=1.2); and $\alpha = H_I^o/1200$.

For wells where no adequate TOC measurements are available, well log curves were used to estimate TOC content. Calibrated by TOC observations from Rock-Eval results, TOC content can then be estimated from petrophysical data using the following linear combination of log curves:

$$TOC = \alpha \log\left(\frac{R_t}{R_{tb}}\right) + \beta(\Delta t - \Delta t_b) + \gamma(GR - GR_b) + \theta(\rho_b - \rho_{bb}) \qquad (2)$$

where α, β, θ, γ are unknown parameters and can be found through curve fitting. R_t and R_{tb} are deep resistivity log and resistivity baseline; Δt and Δt_b are sonic transit time and sonic baseline; GR and GR_b are the Gamma Ray (GR) log and GR baseline; and ρ_b and ρ_{bb} are the bulk density log and density log estimated baseline.

The models from equations (1) and (2) were calibrated using TOC observations from the laboratory results of Rock-Eval analysis and applied to each well. Because the thickness of the Macasty Formation is usually less than 100 metres, the impact of thermal maturity on TOC estimate in each well is limited. Thus, the empirical expression in equation (2) is a simplified version of the revised Passey model (Passey et al., 1990) by Wang et al. (2016). The introduction of Gamma Ray and density logs as compared with the original Passey method can improve the TOC prediction. Figure 22 compares the values from Rock-Eval and well-logs estimated TOCs for DZ006 and D020 wells. The first and third columns in Figure 22 are measured and estimated TOCs, and GR curves are provided in second and fourth columns for the two wells respectively. Comparison of the TOC and GR curves shows a similarity between these two, indicating GR is a good indication of TOC content in the Macasty Formation. Figure 23a and b display organic porosity estimates against initial and measured TOCs respectively. Depending on the maturity and richness of organic matter, the organic porosity could be up to 6 to 7%. The mean of the predicted organic porosity is 2.28% and median 2.44% in the Macasty Formation.

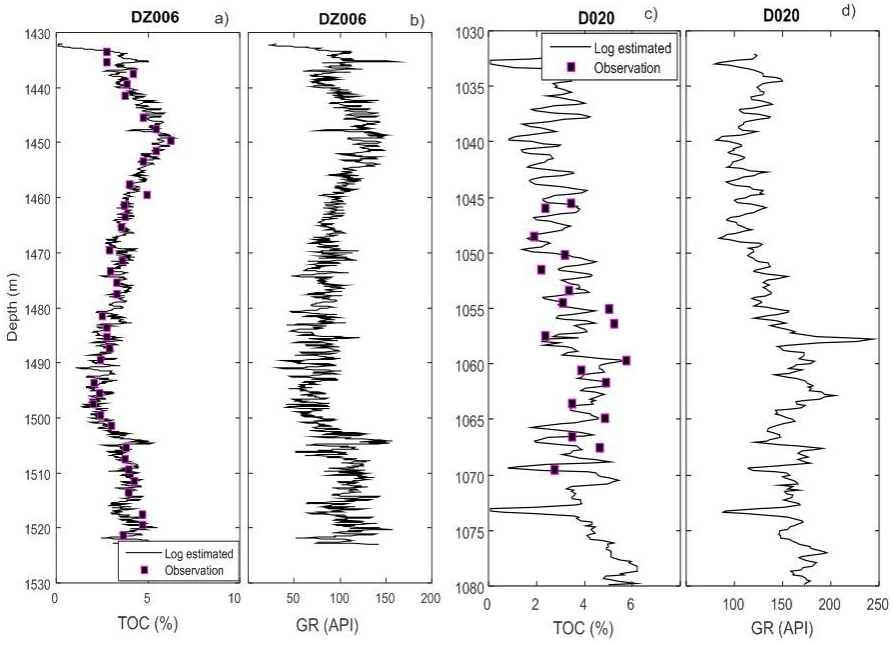

Figure 22: a and c) Measured TOCs of core samples from Macasty Formation in DZ006 and D020 wells by Rock-Eval as compared with estimated TOCs using the revised Passey et al. (1990) method (curve). The unknown parameters in equation (2) for each well were calibrated from TOC measurement in the Macasty interval. b and d) corresponding gamma ray curves to illustrate the direct correlation with the Passey curve.

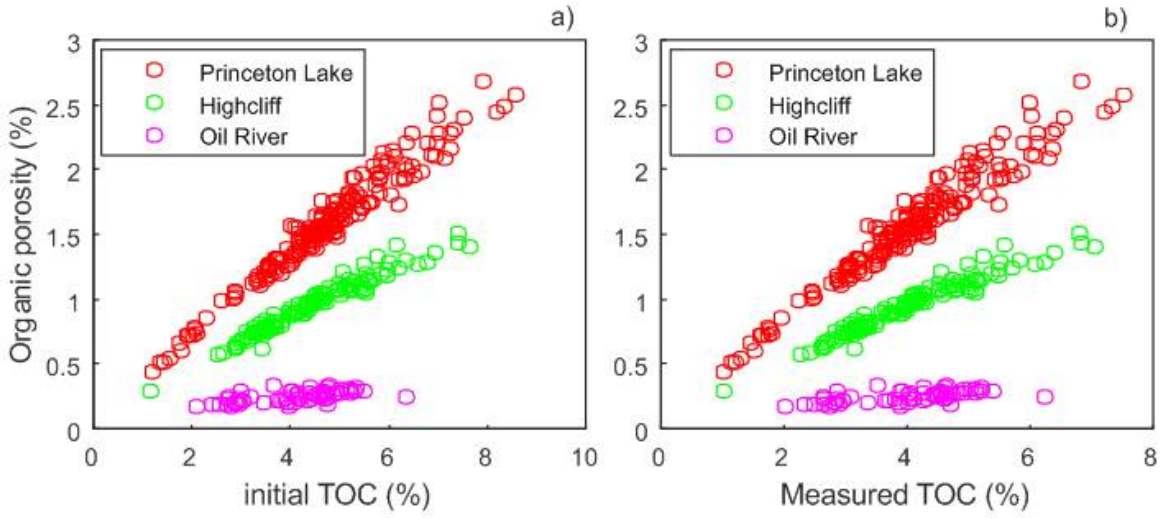

Figure 23: Plots of estimated organic porosities, from Rock-Eval dataset of the Macasty Formation for selected wells, with a) initial and b) measured TOC values.

Reservoir parameters

Laboratory physical measurements (TOC, porosity/permeability) have insufficient spatial coverage and limited vertical resolution, well logs form a complimentary dataset for establishing reservoir parameters based on the various empirical relationships presented before. Well logs data were also used to identify intervals with hydrocarbon resources and to evaluate thicknesses of hydrocarbon bearing intervals in the shale succession. Laboratory measurements of reservoir parameters were used to calibrate various reservoir models.

Figure 24 is an example showing the reservoir parameters of DZ019 based on laboratory and well logs measurements. Considering the fact that pore size is predominantly nanometer scale in shale, a higher hydrocarbon saturation threshold (S_{HC}>60%) is chosen for calculating the net-pay thickness (Figure 24c). The net pay thickness is calculated by summation of all intervals with hydrocarbon saturation higher than 60% and hydrocarbon saturated porosity >2% in the Macasty Formation. There are two potential effective reservoir intervals separated by a low hydrocarbon saturation interval (Figure 24c). Estimated net-pay thicknesses calculated from hydrocarbon exploration wells with data are listed in Table 1.

Figure 25 shows cross plots of resistivity against sonic travel time of selected wells drilled in the Jupiter Fault area to demonstrate graphically the principle in the determination of water saturation (Passey, 1990). From those plots, it can be seen that in most cases, reservoir intervals with high hydrocarbon saturation (high resistivity) are located near or at the top of the Macasty Formation as indicated by yellow colored data points of low resistivity readings dominating at depth.

Well log data were also used to identify potential zones containing oil and gas resources and to estimate net pay thickness in the shale interval. The Arco #1 well (D007) is the deepest well in the area. High Gamma Ray readings, confirmed by high TOC measurements (mean of 2.6% at maturity level of $\%VRo_{equi}$ of 1.6%), indicate an organic rich interval in the Macasty Formation. Large anomalous ΔlogR (Passey et al. 1990, Passey et al, 2010) indicates potential hydrocarbon accumulations (columns 2 and 3 of Figure 26), while a neutron and density porosity cross-over with large ΔlogR anomalies suggest that gas dominates the 2408 to 2438 m interval and that oil is possibly present in the lower part of the formation.

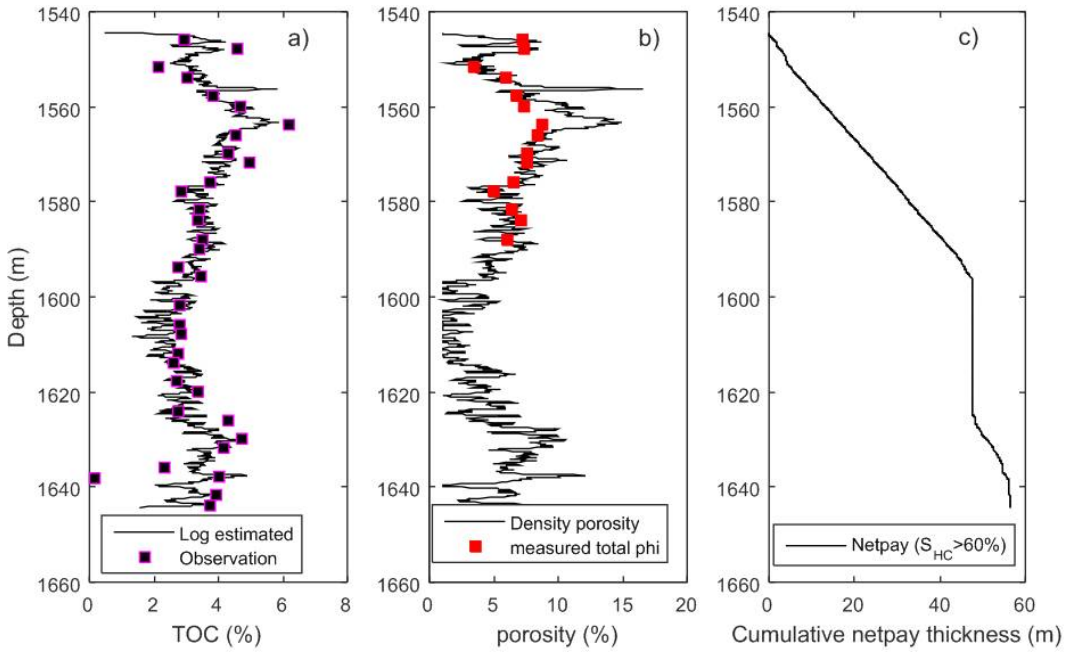

Figure 24. Diagrams showing a) observed and measured TOC contents; b) laboratory measured matrix porosity and estimated log porosity from density; and c) cumulative net-pay thickness by criterion of hydrocarbon saturated porosity greater than 60%. DZ019 well.

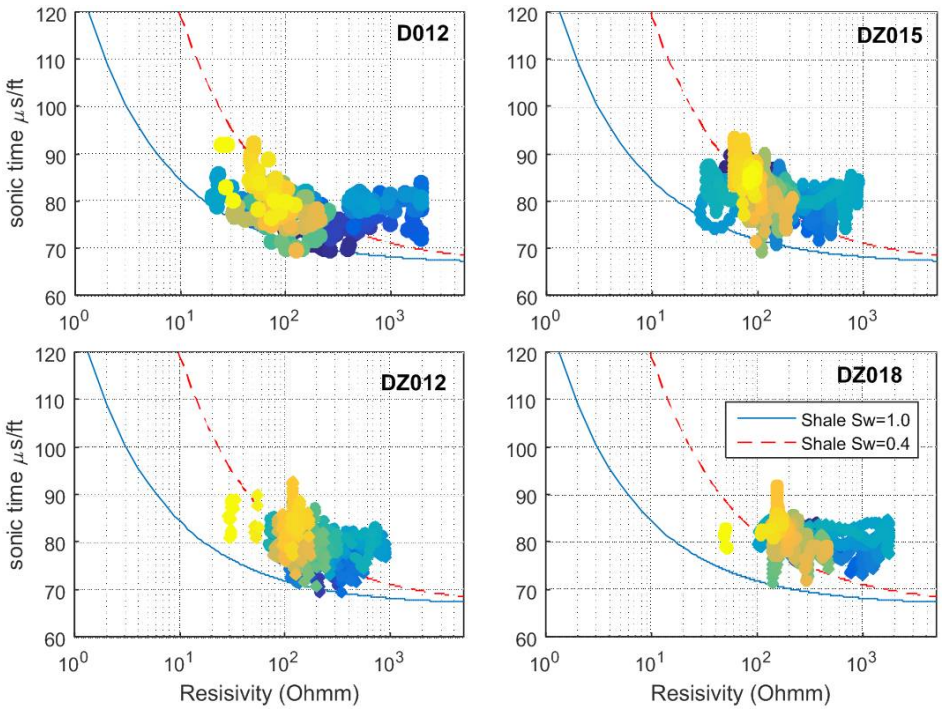

Figure 25. Resistivity-sonic cross plot showing water saturated shale baseline (blue line) and the water saturation of 40% (or S_{HC}=60%; red line) for some wells drilled in the Jupiter Fault area. The color coding indicates relative depth in the Macasty Formation, blue is for shallow and yellow for the deep data.

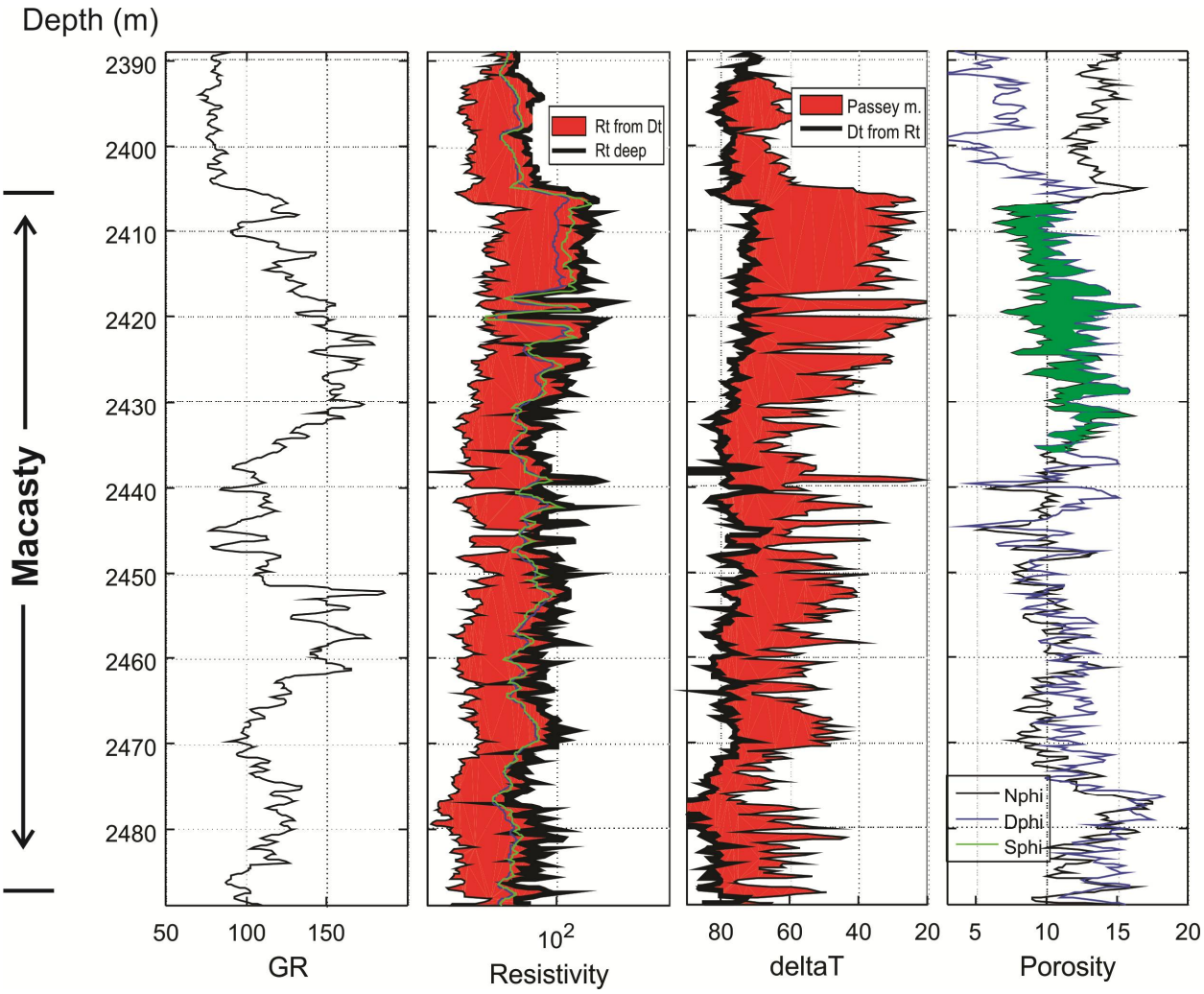

Figure 26: Diagrams showing well log responses and petrophysical anomalies of the potential oil and gas zones in the Macasty Formation in Arco Anticosti #1 well (D007). First column: Gamma Ray log, 2nd column: Resistivity logs and difference between deep resistivity and sonic converted resistivity (filled red) (Passey et al., 1990); 3rd column: Sonic transit time and difference between deep resistivity and sonic converted resistivity (filled red); 4th column: Density and neutron porosities crossover (green fill), an indication of gas reservoir. Nphi: Neutron porosity, Dphi: Density porosity.

Large anomalous ΔlogR in the Macasty Formation from Chaloupe No.1 (D020) well is also observed (Fig. 27, columns 2 and 3), suggesting the presence of potential hydrocarbon. The presence of free hydrocarbon is confirmed by the large number of core sample with high S1/TOCx100 > 100 (Fig. 19a). A mean HI of 558 mg HC/g TOC and Tmax 437°C suggest relative low maturity in an early oil generation window. Without obvious neutron-density porosity cross-over (Fig. 27, column 4), this is consistent with the oil window thermal maturity level.

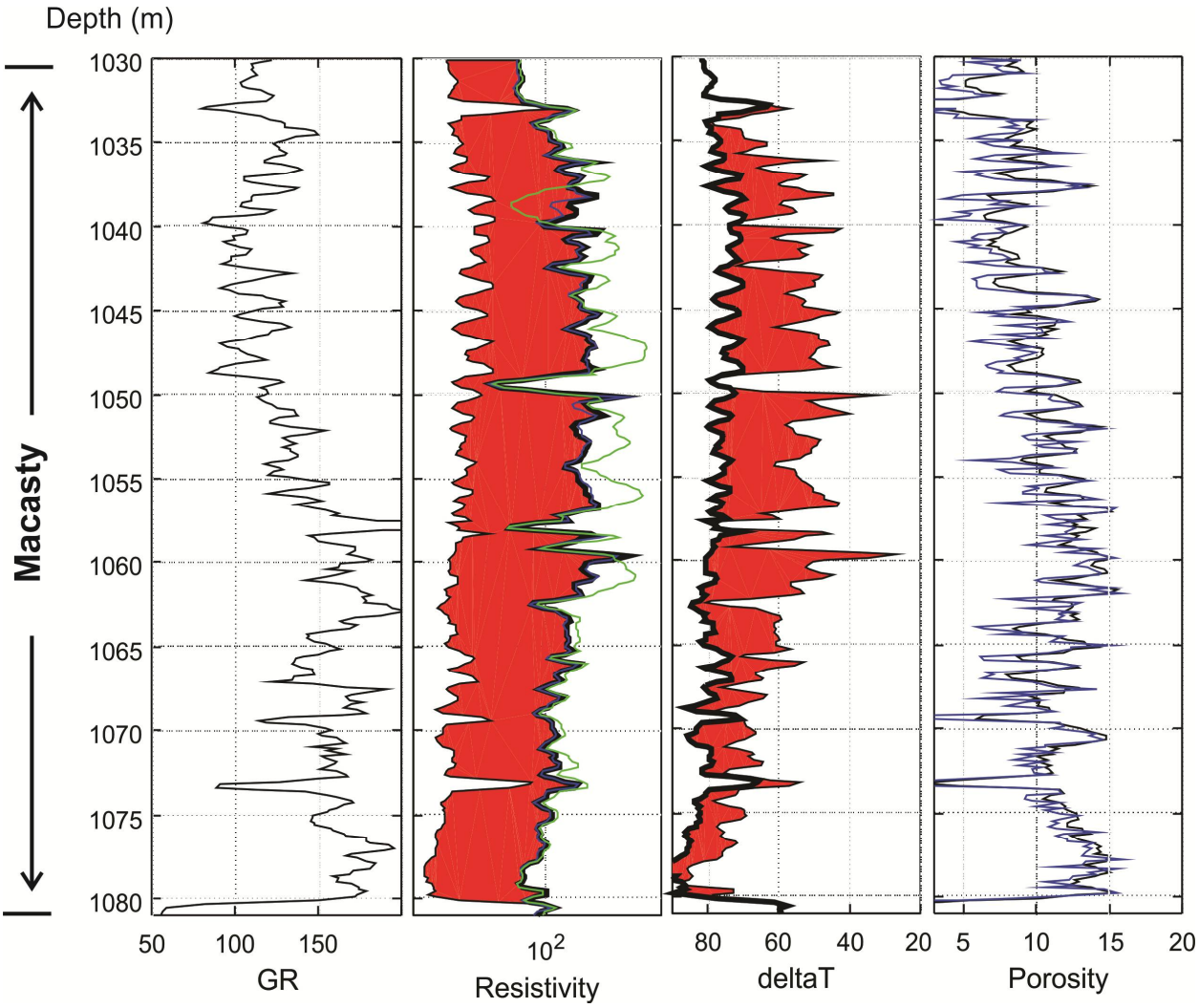

Figure 27. Well log responses and petrophysical anomalies of Macasty Formation in Chaloupe No.1 (D020), Anticosti Island. First column: Gamma Ray log, 2nd column: Resistivity logs and difference between deep resistivity and sonic converted resistivity (filled red) (Passey et al., 1990); 3rd column: Sonic transit time and difference between deep resistivity and sonic converted resistivity (filled red); 4th column: Nphi (black): Neutron porosity, Dphi (blue): Density porosity.

The Shell et al. Roliff #1 (D012) well has high GR readings with an average TOC values of 5.11% suggesting an organic rich shale for the Macasty Formation in this well. Large anomalous ΔlogR indicates potential hydrocarbon presence (Fig. 28). Although no obvious neutron-density porosity cross-over, the two curves move toward each other, suggesting that the hydrocarbon in this well is predominantly liquid with small amount of gas. Well log data analysis indicates that several recent Anticosti Hydrocarbon exploration core holes exhibit obvious anomalies in resistivity and sonic logs in organic rich intervals. Figure 29 is an example from DZ018 showing the general characteristics of well logs and petrophysic anomalies in the Jupiter Fault area. Lack of obvious density-neutron porosity cross-over is common in all wells with the Macasty Formation at shallower depth, suggesting that those wells

are possibly still in the oil generation window, which is consistent with the thermal maturity level based on indicators of Tmax and $\%VRo_{equi}$.

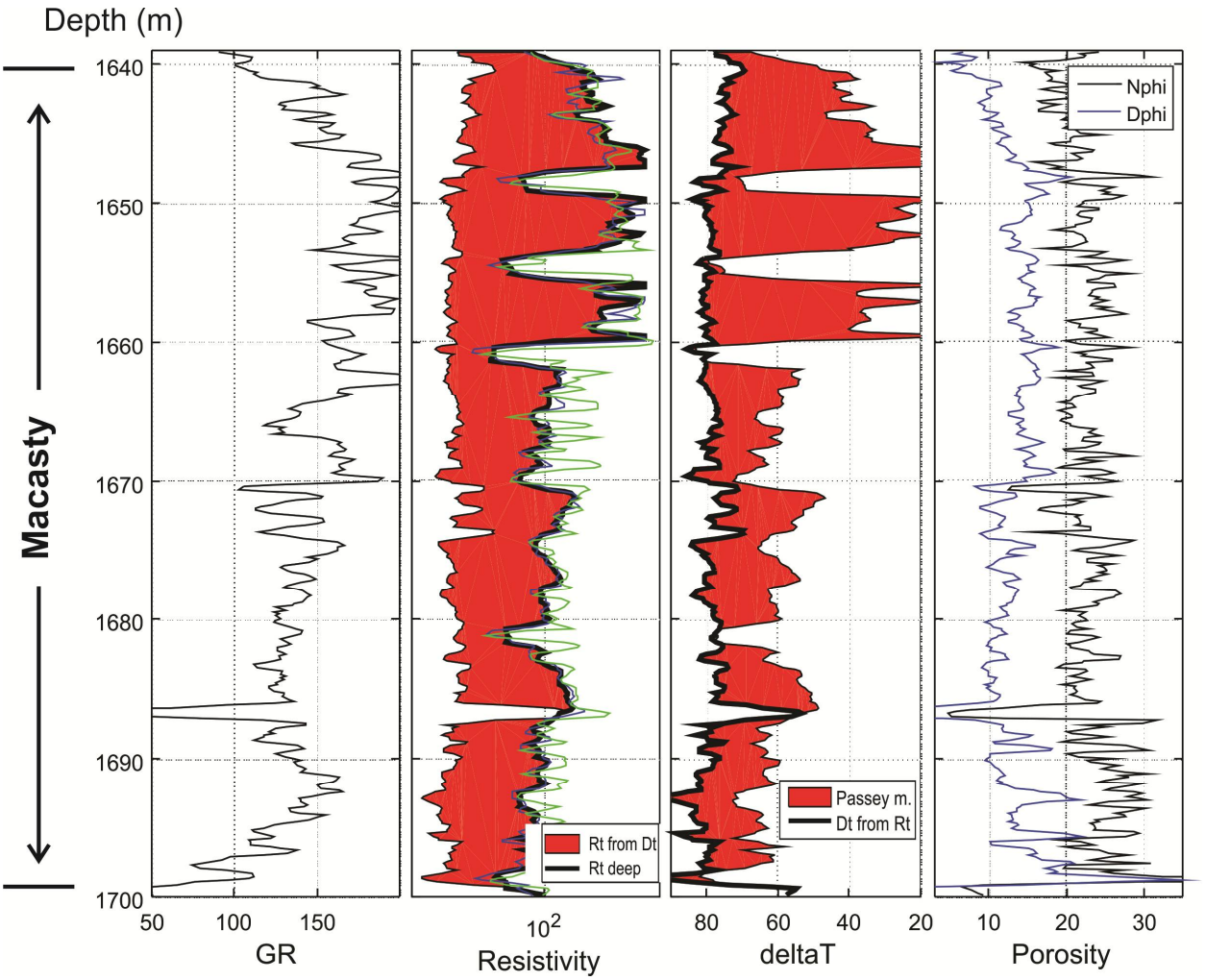

Figure 28: Well log responses and petrophysical anomalies of the Macasty Formation in the Shell-Encal-Corridor Anticosti Roliff #1 (D012) well, Anticosti Island. First column: Gamma Ray log, 2nd column: Resistivity logs and difference between deep resistivity and sonic converted resistivity (filled red) (Passey et al., 1990); 3rd column: Sonic transit time and difference between deep resistivity and sonic converted resistivity (filled red); 4th column: Nphi: Neutron porosity, Dphi: Density porosity.

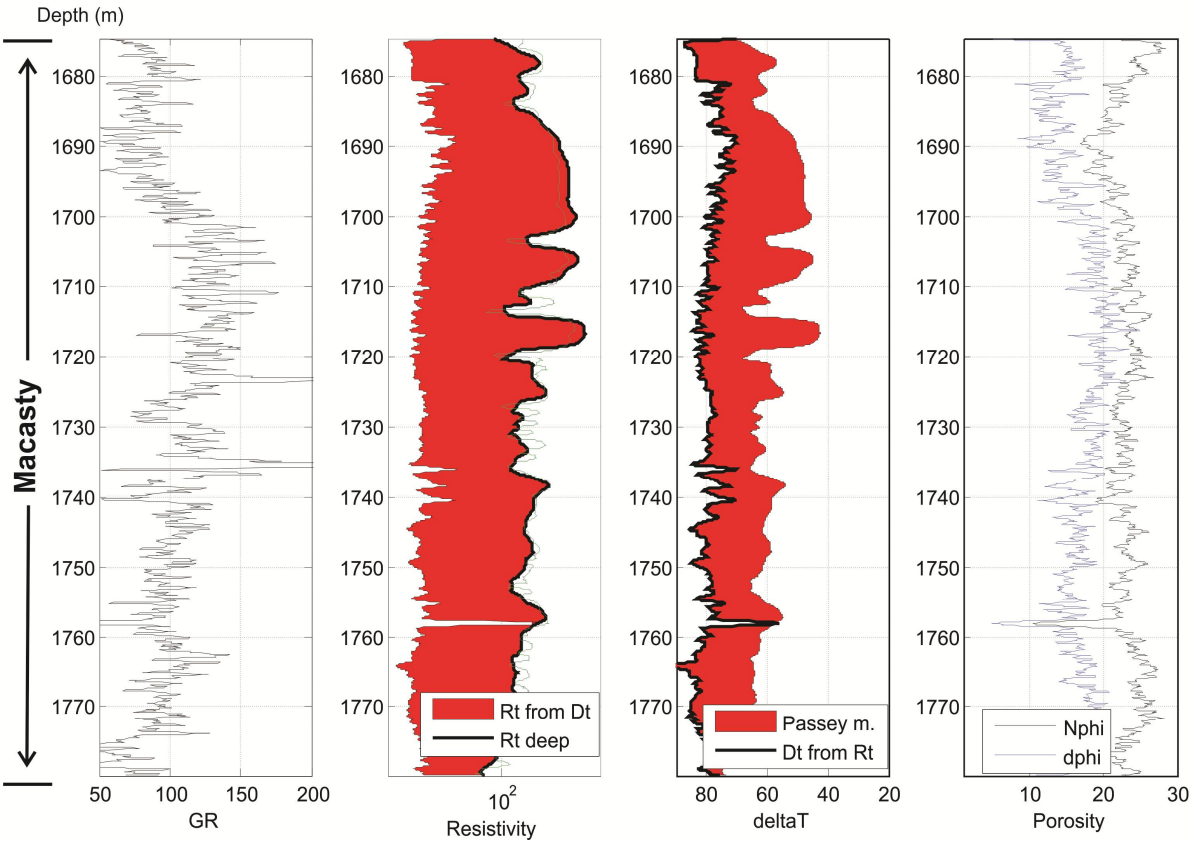

Figure 29. Well log responses and petrophysical anomalies of the Macasty Formation in HASEC Roliff Graben No1 (DZ018), Anticosti Island. First column: Gamma Ray log, 2nd column: Resistivity logs and difference between deep resistivity and sonic converted resistivity (filled red) (Passey et al., 1990); 3rd column: Sonic transit time and difference between deep resistivity and sonic converted resistivity (filled red); 4th column: Nphi: Neutron porosity, Dphi: Density porosity.

Interpretations of acoustic borehole images suggest that there are natural fractures in the Macasty Shale. The interpreted fractures show predominantly horizontal or sub-horizontal with a subsidiary group being either sub-vertical or at high angle with bedding in the study area. The fractures density varies between various core holes. Figure 30 shows an example of high angle fractures (dip >85^o) in DZ015 well and Figure 31 provides an examples of low angle fractures in DZ012 well (dip <35^o). The presence of natural fractures can improve the quality of the source rock reservoir by increasing the capacity of storage and reservoir permeability. This also may indicate that the laboratory measurements may underestimate the porosity and permeability because the scale of natural fracture is far greater than the grain-size of crushed samples.

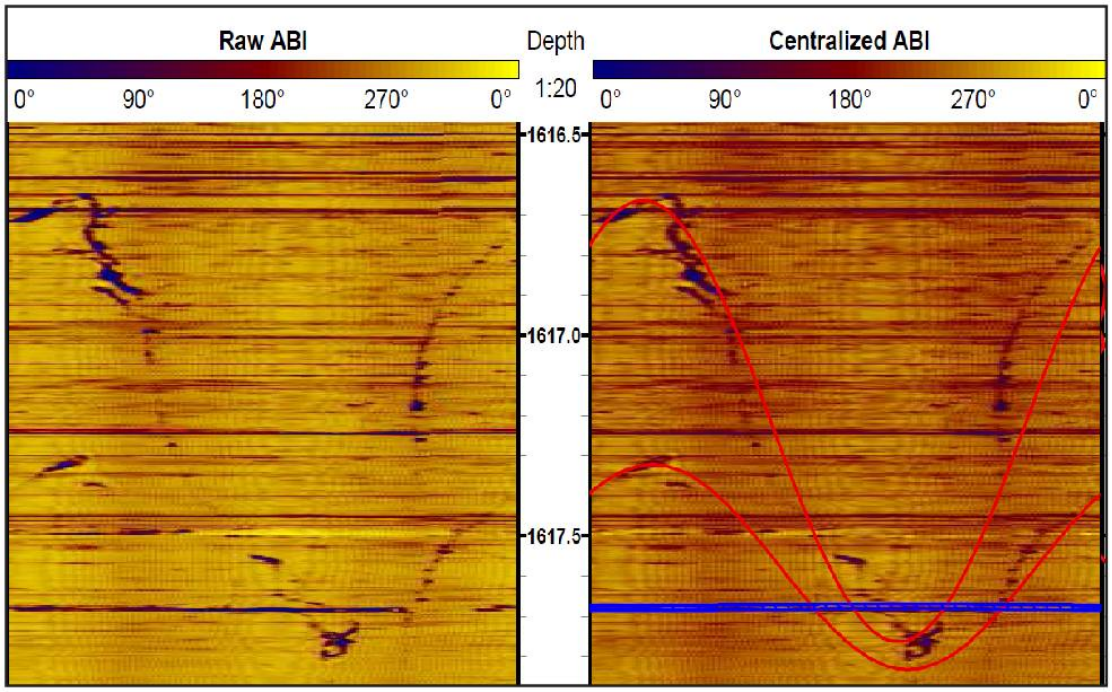

Figure 30. Acoustic borehole image (DZ015 well and depth range 1616.5-1617.85m) showing natural fractures from acoustic anomalies (blue areas on left) and fracture interpretation (red lines on the right). Presence of natural fractures provides more pore space and better permeability for hydrocarbon accumulation and fluid flow in tight source rock reservoir.

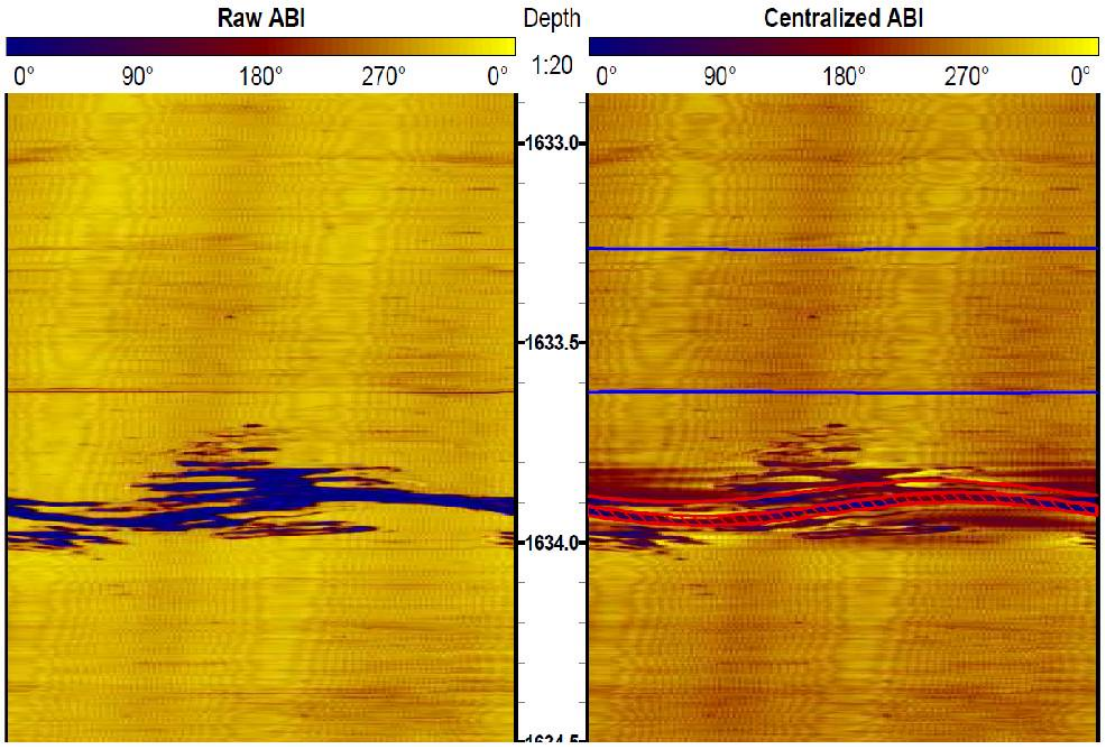

Figure 31 Acoustic borehole images from DZ012 well (1632.8 -1634.5 m) showing the acoustic anomalies (blue areas on left) and fracture interpretation (red lines on the right).

Assessment Results

The hydrocarbon saturated porosity is the sum of hydrocarbon saturated matrix and organic porosities. Figure 32a is a krigged map of the hydrocarbon saurated porosity. The highest values of hydrocarbon saturated porosity are found in the western par tof the island. The Figure 32b is a krigged map of the hydrocarbon pore volume of the Macasty Shale based on a total of 21 wells with available required log data for volumetric parameter estimation. This map shows the spatial variation of the potential hydrocarbon pore volume under reservoir conditions. The geostatistical data analysis suggests a better continuity of the hydrocarbon pore volume in a NW-SE direction, in agreement with the geology of Anticosti island.The estimated hydrocarbon satrurated porosity and pore volume at each well location are indicated in Figure 32 by the color code on the right side.

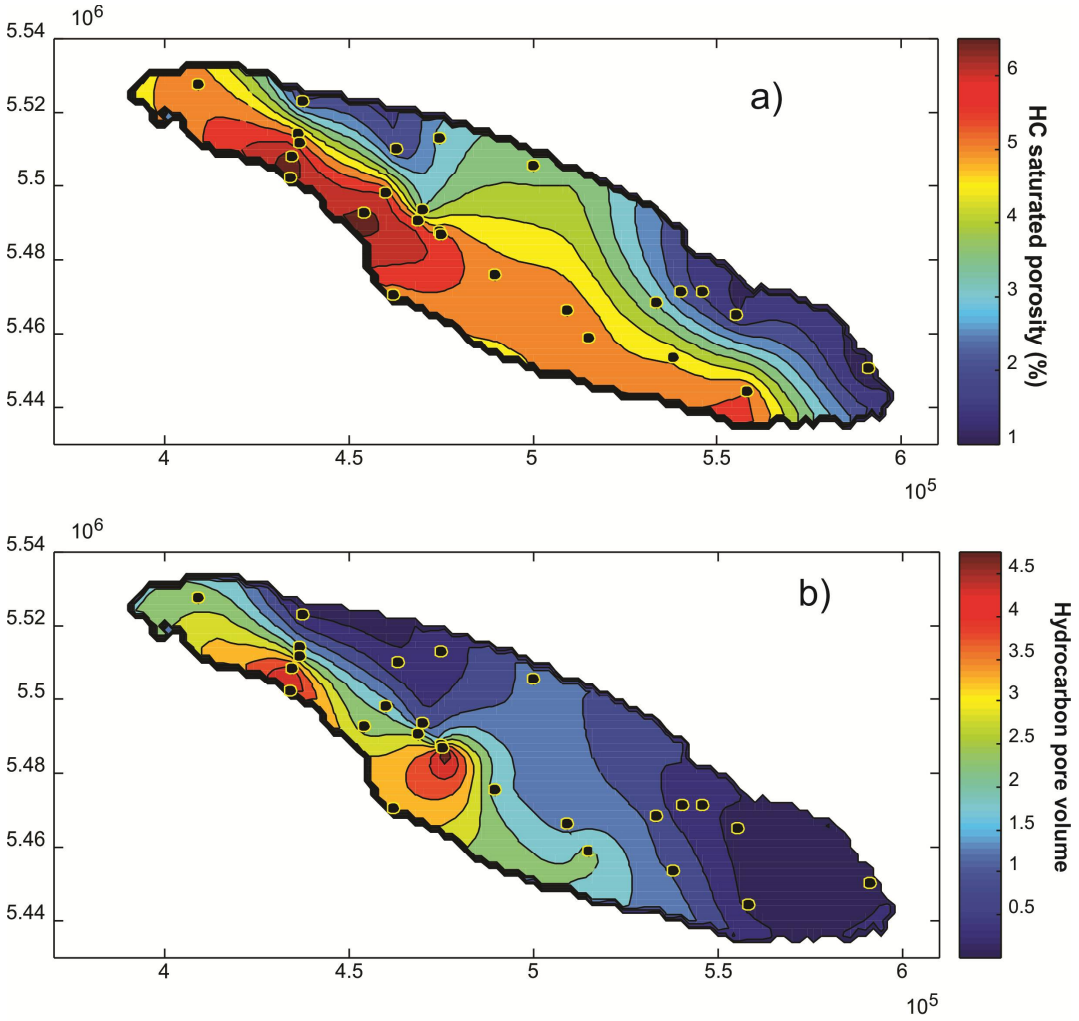

Figure 32. Krigged maps of reservoir volumetric parameters: a) estimated hydrocarbon saturated porosity of the source rock reservoir (%); and b) hydrocarbon pore volume of the source rock reservoir (in million m3/km2). Black dots are control wells. Longitude (UTM) along horizontal axis; latitude (UTM) along vertical axis.

The estimated hydrocarbon pore volume was then divided into oil and gas pore volumes based on a model utilizing S1 evaporative loss in the source rock and the kinetics behaviors characterized by HI decreasing trend with increasing Tmax. By incorporating observed geochemical evidence, such as hydrocarbon in samples, types of organic matter and level of thermal maturity, the model calculates the ratio of oil and gas retained in the source rock reservoirs. The oil and gas pore volumes in reservoir condition were then converted into the in-place oil and gas volumes at standard surface condition by reservoir engineering equations (Chen et al. 2014). The assessment resulted in four different in-place resources: oil, free-gas, dissolved gas (solution gas) and adsorbed gas. The three gas components are then aggregated into total gas using a Monte Carlo algorithm. Positive correlation among the three types of gas components were assumed in the aggregation for two reasons: a) all gases come from the same source rock; and b) thermal maturity has a similar control on all three. Statistic distribution is used to describe the uncertainty in the estimated resource potentials. Our best estimate (the median value or P50, which is the probability that the in-place volume is higher or equal to that estimated at 50%) serves as basis for comparison with best median estimates released by the operators on the island. It should be mentioned that once correlations among variables are introduced in the aggregation, the statistical summations of all percentiles are no longer equal to the simple summations of the three. Mathematical formulation and details of methodology description for calculating different resource components have been discussed in Chen et al. (2014). Method for aggregation of correlated variables is referred to Chen et al., (2012).

The estimated in-place oil resource is shown as statistical distributions graphically in Figure 33 and numerically in Table 7, which demonstrate the range of uncertainty for the oil resource potential evaluation. The oil resource potential evaluation varies from 17.4 (P95) to 55.1 (P5) billions of barrels (Bbls) with a median (P50) of 32.2 Bbls. No attempt is made to estimate the technically recoverable portion of the in-place resources and thus convertible into reserves.

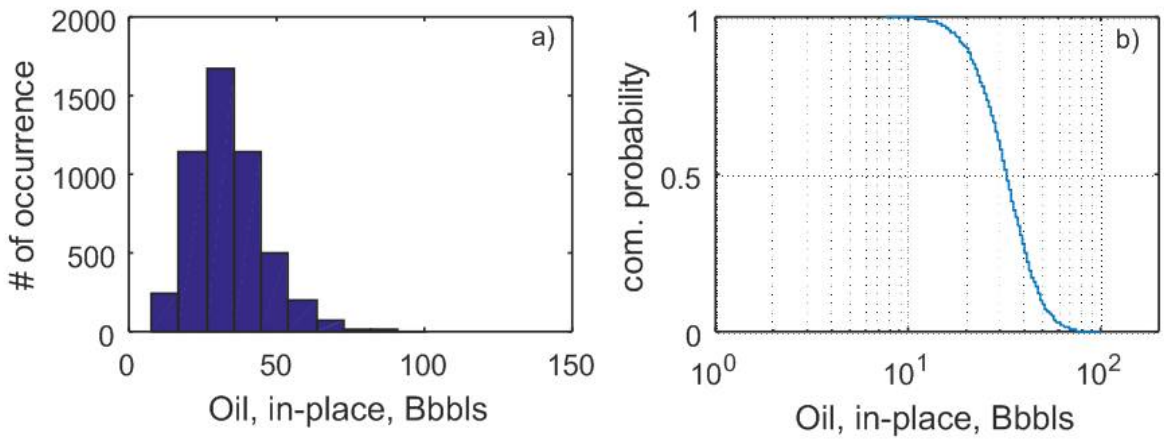

Figure 33: Diagrams showing statistical distributions of estimated in place oil resource in the Macasty Formation of Anticosti Island, a) histogram and b) cumulative distribution based on 5000 Monte Carlo simulations.

Probability	95%	90%	75%	50%	25%	10%	5%
Oil, in-place (Bbbls)	17.4	20.4	25.5	32.2	40.3	48.8	55.1
Total gas in-place (TCF)	29.6	34.5	41.4	51.2	63.5	76.5	83.4
Total oil eq (Bboe)	23.1	26.6	32.6	40.6	50.4	60.6	66.7

Table 7. Summary of potential oil and gas in-place resources in the Macasty Formation as cumulative distribution.

The spatial distribution of the estimated oil resource is presented as an oil resource density map (Fig. 34) to outline the geographical location of potential “sweet-spots” of the oil resource in the Macasty Formation. The oil resource in the Macasty Formation occurs primarily in the northwestern and central parts of the Island, where the source rock is still in the oil generation window with a thick organic-rich Macasty Formation. On the other hand, the southeastern and northeastern sectors are characterized by a much lower in-place oil resource potential.

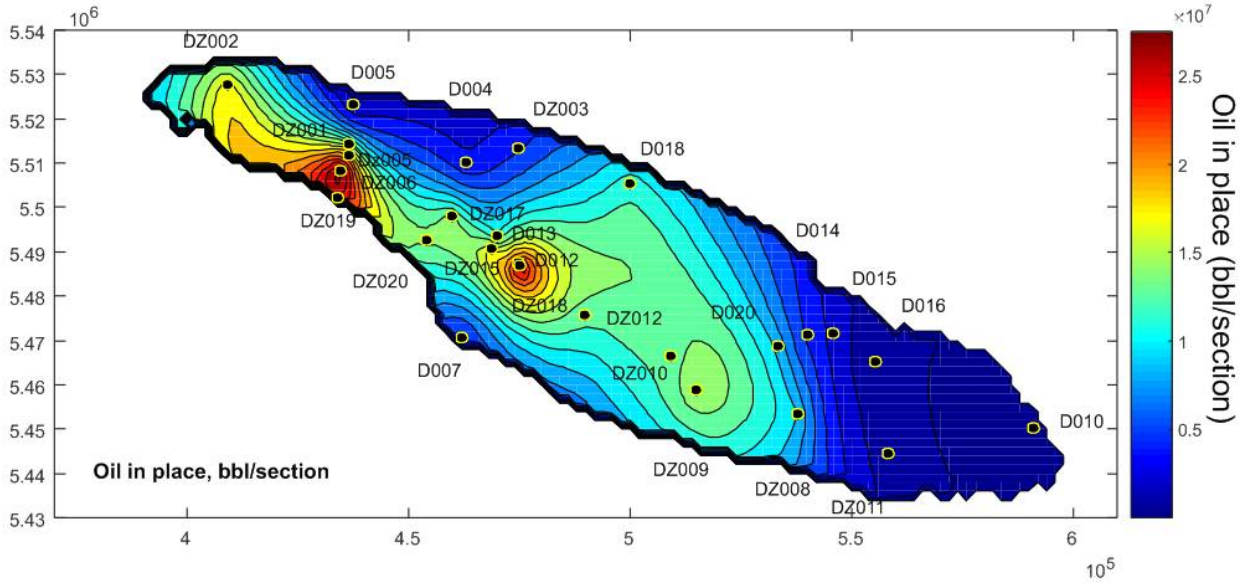

Figure 34: Oil resource (in-place) density map showing spatial distribution of the predicted oil resource in the Macasty Formation. Longitude (UTM) along horizontal axis; latitude (UTM) along vertical axis. bbls/section : barrels (x10^7) per square mile (section).

Figures 35 and 36a are the results of the aggregated total natural gas in the Macasty Formation. The median (P50) resource value of the total gas in-place is 51.2 TCF with an uncertainty range from 29.6 TCF (P95) to 83.4 TCF (P5) (Table 7). Because the Macasty Formation in most of the assessed area is still in the oil generation window, natural gas is primarily from solution gas. Adsorbed gas and free gas only account for about 30% and 10%, respectively (Figure 36a). The geographic variation of the total natural gas (in-place) is depicted on a resource density map in Figure 37. The northwestern region and southwestern area around the Arco Anticosti # 1 well (D007) appear to contain more gas resources in the Macasty Formation. It is noteworthy that similarly with the evaluation of the in-place oil resource, the southeastern and northeastern sectors of the island contain a significantly interpreted lower volume of in-place natural gas.

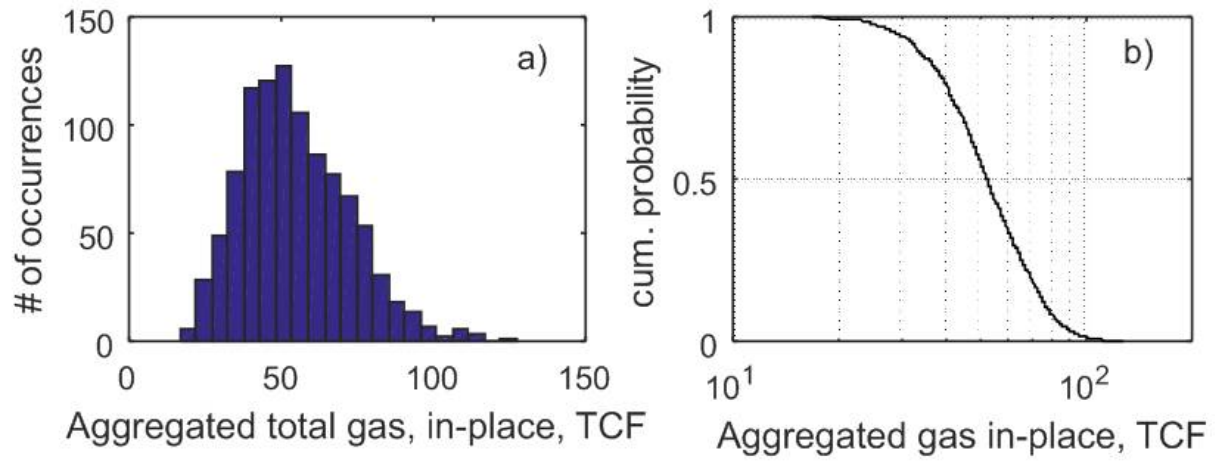

Figure 35. Statistical distributions of the aggregated natural gas in-place. A histogram (a) and cumulative distribution (b).

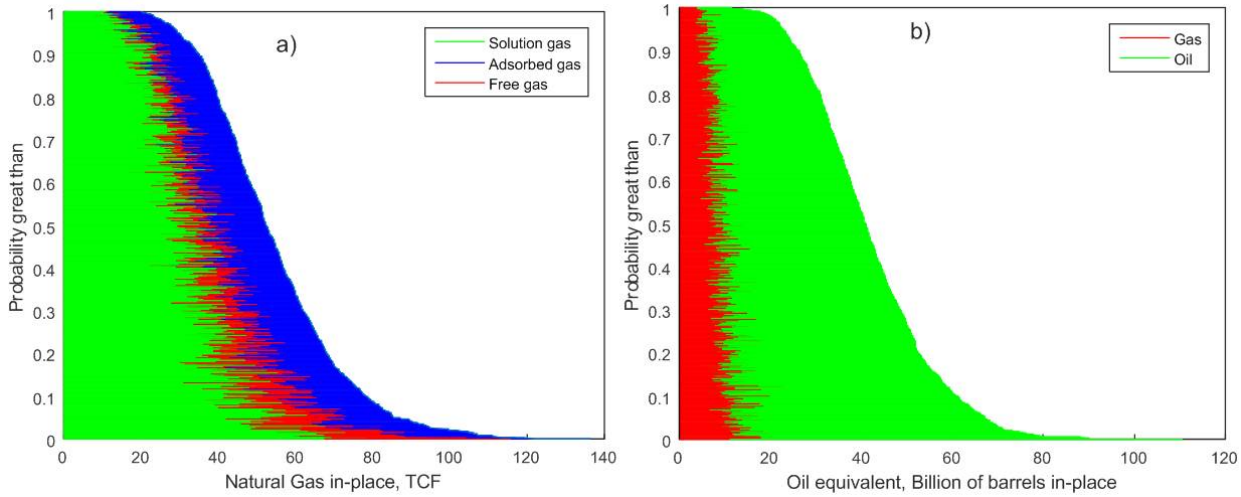

Figure 36: Cumulative distribution of aggregated total natural gas and oil equivalent in-place resources showing relative abundances of different gas components (a) and oil and gas (b).

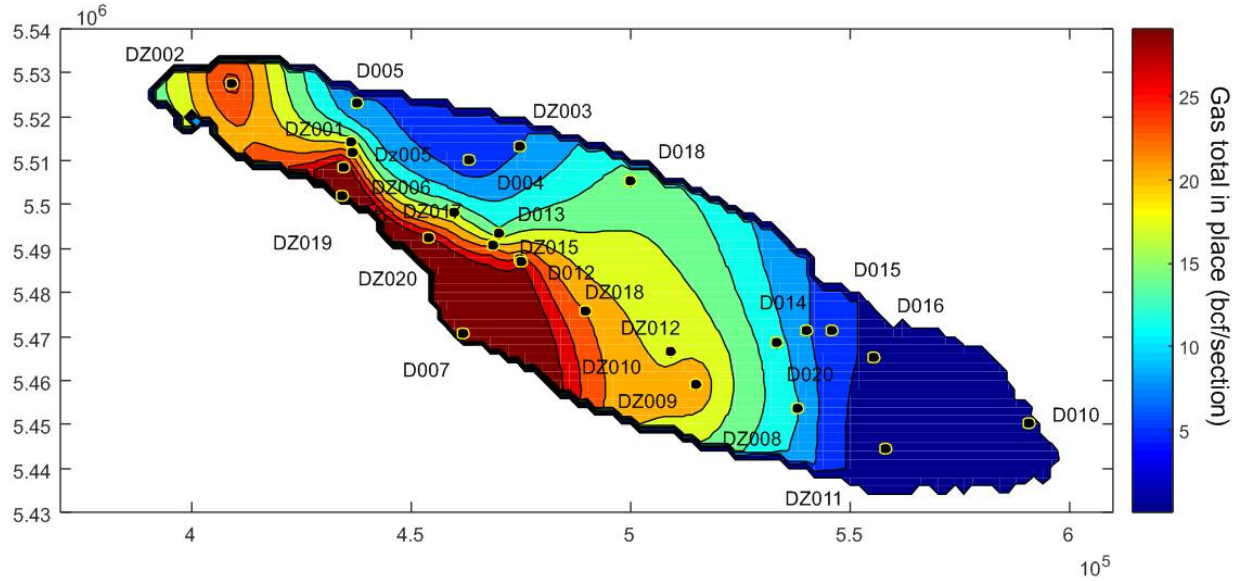

Figure 37: Geographic distribution of natural gas resource in Macasty Shale of the Anticosti Island. Longitude (UTM) along horizontal axis; latitude (UTM) along vertical axis. Bcf/section; Billions of cubic feet per square mile (section).

From Table 7 and the diagrams of statistical distribution of various resource estimates, it is clear that there are substantial uncertainties in the resulting resource potential estimates because of sparce data coverage, discrepencies in thermal maturity data and lack of information with respect to reservoir fluid properties and pressure-volume-temperature subsurface conditions. Those uncertainties in the data are translated into the large uncertainties in hydrocarbon volume estimates and type prediction.

DISCUSSION

This study is the first independent evaluation of the in-place unconventional hydrocarbons (oil and gas) on Anticosti Island. The study is based on a methodology developed by the Geological Survey of Canada to evaluate the resource potential in shale and tight reservoir succession. The evaluation is based on available data (well-logs, organic and mineral geochemistry) in the public domain and from the confidential data from the operators on the island (Anticosti Hydrocarbons Consortium and Junex).

The sparse distribution of wells on the island (1 well/200 km^2) and the variations in the density, nature and type of available data result in a wide uncertainty ranges of the evaluation results (Table 7). In comparison, the Horn River Basin in northeast British Columbia has a surface area (7800 km^2) roughly similar to that of Anticosti island (7900 km^2), but with a number of wells ten time higher (376 so 1 well/20 km^2) and historical production data. This abundance of geoscientific and technical data, allow a more reliable evaluation of the in-place resources and consequently of the recoverable resources, but also

serves to identify areas richer in hydrocarbons or "sweet spots" in terms of productivity and recoverability for resource development planning and investment decisions.

This study provides in-place oil and gas resource estimates, but does not evaluate the technical recoverable resources, nor the economic feasibility of their eventual development. This study evaluates that the best estimate (P50, or the probability that the in-place volume is higher or equal to that estimated at 50%) in-place hydrocarbon resources on Anticosti island is 32.2 billion oil barrels (Bbls) and 51.2 trillions of cubic feet (TCF) of gas. These best estimate values would equate to 40.6 billion of oil equivalent barrels (BBOE) (at a ratio of thermal equivalence of 6000 cubic feet of natural gas for 1 oil barrel). From these results, a ratio of 79% oil versus 21% natural gas would be present on Anticosti island. The best estimate in-place resource (oil and gas) on the island is 5.1 MBOE/ km^2 (millions of barrels of oil equivalent per km^2) or 13.3 MBOE/section (or square mile).

The recent industry evaluations on the in-place resources o Anticosti Island were reported in BBOE. The study by Sproule (for Hydrocarbon Anticosti: 6070 km^2 or 77% of the island superficies) [*] suggested the presence at P50 of 30.7 BBOE (range of 20.9 BBOE at P90 and of 45.2 BBOE at P10) and the NSAI study (for Junex acreage: 1264 km^2 or 16% of the island superficies) indicate the presence at P50 of 12.2 BBOE (range of 10.2 BBOE at P90 and 14.4 BBOE at P10). Thus a P50 total of 42.9 BBOE would be present on the island from previous industry evaluation, a value similar to our evaluation. It should be noted that the average in-place resources per km^2 is higher in the NSAI report (9.6 MBOE/km^2) compared to the Sproule report (5.1 MBOE/km^2). That variation is likely related to the fact that a thicker and overpressured succession occurs in the Junex acreage and this is confirmed by the geographic distribution of the in-place natural gas resource shown on Figure 37. For most of the producing basins, the in-place resource is expressed in resource volume per section (square mile). In the case of Anticosti, based on previous reports, the Hydrocarbon Anticosti acreage contains 13.2 MBOE/section and that of Junex contains 25 MBOE/section.

Table 8 compares the in-place resources at P50 for some shale basins in North America (Milici, 2005; Jarvie, 2012b; Rokosh et al., 2012; Wickstrom, 2013; Chen et al., 2014; Corridor Resources, 2014; US EIA, 2011, 2013). This table should not serve as a tool to evaluate the economic potential of specific shales as it includes plays with only gas and plays with mixed oil and gas. The interest of this table is to compare the density of the in-place resource reported in equivalent barrels. Readers should note that we do not present data for unconventional tight siltstone or sandstone (e.g., Bakken and Montney formations) which are different resource plays. The basin area consists only of the proven and prospective area of these basins.

[*] The Vauréal National Park is 572km^2 or 7% of the island

Shale unit	Age	Basin area (km^2 - mi^2)	Oil (BBls) - Gas (TCF)	Barrels equivalent (BBOE)	Density In-place MBOE ($/km^2$ - $/mi^2$)
Macasty (QC)	**Late Ordovician**	**7900 - 3050**	**32.2 - 51.2**	**40.6**	**5.1 - 13.3**
Utica (QC)	Late Ordovician	10000 - 3861	1.9 - 176	31.2	3.1 - 8.1
Utica / Point Pleasant (OH)	Late Ordovician	58300 - 22500	110 - 314	162.3	2.8 - 7.2
Horn River Shales (BC)	Middle Devonian	8600 - 3320	0 - 530	74.7	6.4 - 16.7
Marcellus (core area; PA)	Late Devonian	53750 - 20750	0 - 1500	250	8.3 - 21.7
Duvernay (AB)	Late Devonian	52700 - 20350	67 - 483	147.5	2.8 - 7.3
Frederick Brook* (NB)	Early Carboniferous	485 - 188	0 - 67	11.2	23.1 - 59.7
Eagle Ford (TX)	Cretaceous	8601 - 3321	33.2-76.8	46	5.3 - 13.9

Table 8. Summary of unconventional in-place resources (oil and gas) at P50 for various Canadian and American shale formations. The evaluated area is for the prospective part of the basin. BBls: Billions of barrels of oil, TCF: Trillion of cubic feet of natural gas, BBOE: Billions of barrels of oil equivalent, MBOE: Millions of barrels of oil equivalent. * Evaluation only done on a limited acreage in the Moncton sub-basin.

The Macasty Formation has a higher in-place resource density compared to the coeval Utica Shale of southern Quebec and Utica / Point Pleasant in Ohio. This average in-place resource density compares well with that of other shale basins mixed resources (oil and gas) such as the Duvernay (Alberta) and the Eagle Ford. However, the average in-place resource density for the gas fields such as the Horn River (British Colombia) and the Marcellus (Pennsylvania) is definitively much higher. It is noteworthy that the in-place resource density for the Frederick Brook Member (Albert Formation) in New Brunswick is relatively much higher compared to other units, although this evaluation only concerns a small area of the Carboniferous basin and no data is available for most of the latter.

Our study did not attempt to evaluate the technical recoverable resource using global analogues of recovery factor as the recovery varies greatly among the shale resource plays. A reliable recoverable resource evaluation would need to have well EUR (estimated ultimate recovery) from a few years of hydrocarbon production to establish statistical trends of production decline. Use of production data from other producing sedimentary basins, identified as analogous on the basis of geological criteria (mineral composition, type of organic matter, thermal history, etc…) is sometimes considered as an alternative for evaluating recoverable resources. This type of approach was followed by the Ministère des finances du Québec who in 2015 has released a study of economic feasibility of potential development of unconventional resources on Anticosti. Their analogues scenario was based on comparisons with the Utica / Point Pleasant field in Ohio and assumed an in-place resource of 42.9 BBOE (data from the industry for Anticosti) with an oil to gas production ratio of 22.5% to 77.5% (Gouvernement du Québec, 2015). This last study hypothesized on a potential development scenario of about 25% of the island where the geological conditions were more favorable, hence focused on areas where the Macasty Formation was

deeper (overpressured) with higher thermal rank and more gas. This oil/gas ratio is totally contrary to our in-place resource results, a difference explained by different ultimate objectives of our respective studies.

CONCLUSIONS

A petroleum resource assessment has been conducted for the Macasty Formation shale reservoir in Anticosti Island of eastern Quebec. A reservoir volumetric method using the dual porosity model developed by the Geological Survey of Canada was used to assess the oil and gas resource potentials based on available geological, geochemical, geophysical and reservoir data. This assessment provides estimates of in-place resource. No effort has been made to assess the technically recoverable resources.

The volumetric calculations suggest that the Macasty Formation contains large volume of in-place hydrocarbon resources. The best estimates (P50) in-place resources include 32.2 billion barrels of oil and 51.2 TCF of natural gas for the entire island. This assessment report also presents the estimates as oil and natural gas resource density maps to illustrate the spatial variations of the predicted oil and gas resources. The assessment indicates substantial uncertainties in the estimated oil and gas resources due to inadequate data coverage, uncertainties in the geoscience data that were used and understanding of the geology in the basin. Those uncertainties are indicated graphically and numerically (Figs. 33, 35 and 36; Table 7) in this report.

ACKNOWLEDGEMENTS

Dr. Keith Dewing of the GSC is thanked for his review of the report, his comments and suggestions are greatly appreciated. We would like to thank Karine Bédard and Félix-Antoine Comeau of the Institut National de la Recherche Scientifique, Eau Terre Environnement center, for the set-up of a 3D model of Anticosti Island, as well as Virginia Brake of the GSC for her technical assistance. Anticosti Hydrocarbons L.P. (Pétrolia inc., Corridor Resources Inc., Saint-Aubin E&P (Québec) inc., and Ressources Québec) are thanked for allowing access to various datasets for the assessment. Junex Resources is thanked for allowing the use of their Rock-Eval dataset and presented, but unpublished material. The Ministère de l'Énergie et des Ressources Naturelles du Québec is thanked for providing us access to all public domain geoscience data in their SIGPEG database. Dr. Xiaojun Liu of GSC assisted for the inversion modeling of kerogen kinetic parameters using available pyrograms.

REFERENCES

Achab, A., Asselin, E., Desrochers, A., Riva, J.F., Farley, C., 2011, Chitinozoan biostratigraphy of a new Upper Ordovician stratigraphic framework for Anticosti Island, Canada. Geological Society of America Bulletin, v. 123, p. 186-205.

Allen, J.S., Thomas, T.A., Lavoie, D., 2009. Stratigraphy and structure of the Laurentian rifted margin in the northern Appalachians: a low-angle detachment rift system. Geology 37, 335–338.

Ambrose, R.J., Hartman, R.C., Diaz-Campos, M., Akkutlu, I.Y., Sondergeld, C.H., 2012. Shale Gas-In Place calculations Part I: New pore-scale considerations. SPE Journal, March, p. 219-229.

Bertrand, R., 1987. Maturation thermique et potentiel pétroligène des séries post-Taconiennes du Nord-Est de la Gaspésie et de l'Ile d'Anticosti. Unpublished D.Sc thesis, Neuchâtel University, 647 p.

Bertrand, R., 1991. Maturation thermique des roches mères dans les bassins des basses terres du Saint-Laurent et dans quelques buttes témoins au sud-est du Bouclier canadien. International Journal of Coal Geology, v. 19, p. 359–383.

Bertrand, R. and Héroux, Y., 1987. Chitinozoan, graptolite, and scolecodont reflectance as an alternative to vitrinite and pyrobitumen reflectance in Ordovician and Silurian strata, Anticosti Island, Quebec, Canada. AAPG Bulletin, v. 71, p. 951–957.

Bordet, E., Malo, M., Kirkwood, D., 2010. A structural study of western Anticosti Island, St. Lawrence platform, Quebec: A fracture analysis that integrates surface and subsurface structural data. Bulletin of Canadian Petroleum Geology, v. 58, p. 36-55.

Brake, V., Pinet, N., 2015. Additional insights on fracture patterns in the northern Anticosti Basin from satellite, aerial and bathymetric images. Geological Survey of Canada, Open File 7911, 21 p.

Cander, H., 2013, Finding Sweet Spots in Shale Liquids and Gas Plays: (with Lessons from the Eagle Ford Shale); Search and Discovery Article #41093, Posted December 10, 2012, May 13, 2013. http://www.searchanddiscovery.com/pdfz/documents/2013/41093cander/ndx_cander.pdf.html

Carr., A.D., 1999. A vitrinite reflectance kinetic model incorporating overpressure retardation. Marine and Petroleum Geology, v. 16, p. 355-377.

Carsted, D.J., Karri, S., Romanov, A., 2011. Resource assessment of the Macasty Formation in certain petroleum and natural gas holdings on Anticosti Island for Petrolia and Corridor Resources Inc (As of 1 June, 2011). 50p. http://www.petroliagaz.com/imports/medias/pdf/rapports-financiers/2011-rapport-51-101-anticosti-en.pdf [last access, January 28, 2016].

Castonguay, S., Wilson, R.A., Brisebois, D., Desrochers, A., Malo, M., 2005. Compilation géologique, Anticosti-Gaspé- Campbellton, les ponts géologiques de l'est du Canada, Transect 4, Québec-Nouveau-Brunswick. Commission Géologique du Canada, Open File 4883, 1:125 000, 4 sheets.

Chatellier, J.Y., Ferworn, K., Larsen, N.L., Ko, S., Flek, P.. Molgat, M., Anderson, I., 2013. Overpressure in shale gas: When geochemistry and reservoir engineering data meet and agree. In: J.Y. Chatellier and D. Jarvie, (eds.) Critical assessment of shale gas resource play. AAPG Memoir 103, p. 45-69

Chen, Z., Osadetz, K. G., Dixon, J. and Dietrich, J., 2012, Using copula for implementation of variable dependencies in petroleum resource assessment: Example from Beaufort-Mackenzie Basin, Canada, AAPG Bulletin, V.96, No.3, pp. 439–457. DOI: 10.1306/06301110196.

Chen, Z., Jiang, C., 2015, A data driven model for studying kerogen kinetics with unconventional shale application examples from Canadian Sedimentary Basins. Marine and Petroleum Geology, v. 67, p.795-803, doi:10.1016/j.marpetgeo.2015.07.004.

Chen, Z., Jiang, C., 2016, A revised method for organic porosity estimation using Rock-Eval pyrolysis data, example from Duvernay Shale in the Western Canada Sedimentary Basin. AAPG Bulletin. V.100, no. 3, p. 405-422. DOI:10.1306/08261514173.

Chen, Z., Lavoie, D., Malo, M., 2014. Geological characteristics and petroleum resource assessment of Utica Shale, Quebec, Canada. Geological Survey of Canada, Open File 7606, 43 p.

Chi, G., Lavoie, D., Bertrand, R., Lee, M.-K., 2010. Downward hydrocarbon migration predicted from numerical modeling of fluid overpressure in the Paleozoic Anticosti Basin, eastern Canada. Geofluids, v.10, p. 334-350.

Desrochers, A., 1988. Stratigraphie de l'Ordovicien de la région de l'Archipel de Mingan. Ministère des Ressources Naturelles du Québec, MM 87-01, 62p.

Desrochers, A., 2006. Rocky shoreline deposits in the Lower Silurian (upper Llandovery, Telychian) Chicotte Formation, Anticosti Island, Quebec. Canadian Journal of Earth Sciences, v. 43, p. 1-10.

Desrochers, A., James, N.P., 1988. Early Paleozoic surface and subsurface paleokarst : Middle Ordovician carbonates, Mingan Islands, Quebec. In: N.P. James, P.W. Choquette, (eds.), Paleokarst. Springer, London, p. 183- 210.

Desrochers, A., Farley, C., Achab, A., Asselin, E., Riva, J.F., 2010, A far-field record of the end Ordovician glaciation: The Ellis Bay Formation, Anticosti Island, Eastern Canada, Palaeogeography, Palaeoclimatology, Palaeoecology, v. 296, p. 248-263.

Desrochers, A., Brennan-Alpert, P., Lavoie, D., Chi, G., 2012. Regional stratigraphic, depositional and diagenetic patterns from the interior of the St. Lawrence Platform: the Lower Ordovician Romaine Formation, western Anticosti Basin, Québec.In J.R. Derby, R.D. Fritz, S.A. Longacre, W.A. Morgan, C.A. Sternbach, (eds.) The great American carbonate bank: The geology and economic resources of the Cambrian - Ordovician Sauk megasequence of Laurentia, Memoir of the American Association of Petroleum Geologists, 98, p. 525-543.

Dietrich, J., Lavoie, D., Hannigan, P., Pinet, N., Castonguay, S., Giles, P., Hamblin, A.P. 2011. Geological setting and resource potential of conventional petroleum plays in Paleozoic Basins in Eastern Canada. Bulletin of Canadian Petroleum Geology, v. 59, p. 54-84.

Dutton S.P., Loucks, R.G., 2010. Diagenetic controls on evolution of porosity and permeability in lower Tertiary Wilcox sandstones from shallow to ultra-deep (200-6700) burial, Gulf of Mexico Basin, USA. Marine and Petroleum Geology, v. 27 p. 69-81.

Espitalié, J., Laporte, J.L., Madec, M., Marquis, F., Leplat, P., Paulet, A., Boutefeu, J., 1977. Méthode rapide de caractérisation des roches mères de leur potentiel pétrolier et de leur degré d'évolution. Revue de l'Institut Français du Pétrole vol. 32, p. 23-42.

Espitalié , J., Marquis, F., Sage, L., Barsony, I., 1987. Géochimie organique du bassin de Paris. Revue de l'Institut Français du Pétrole, v. 42, p. 271–302.

Goodarzi, F. 1985. Reflected light microscopy of chitinozoan fragments. Marine and Petroleum Geology, v. 2, p. 72–78.

Goodarzi, F., Norford, B.S., 1985. Graptolites as indicators of the temperature histories of rocks. Journal of the Geological Society of London, v. 142, p. 1089–1099.

Gouvernement du Québec, 2015. Évaluation financière, évaluation des retombées économiques et scénarios possibles de développement de l'exploitation d'hydrocarbures sur l'île d'Anticosti. Évaluation environnementale propre à Anticosti, Chantier Économie, Rapport AECN01-AECN02, 98 p.

Hartkopf-Fröder, C., Königshof, P., Littke, R., Schwarzbauer, J. 2015. Optical thermal maturity parameters and organic geochemical alteration at low grade diagenesis to anchimetamorphism: A review. International Journal of Coal Geology, v. 150–151, p. 74–119.

Hunt, J.M., 1996. Petroleum Geochemistry and Geology. W.H. Freeman and Company, New York (743 p.).

INRS-Pétrole, 1974. Potentiel pétrolier du sondage ARCO-Anticosti no. 1 (49°23'18'' - 63° 31'29''; 12583 pieds). Étude sédimentologique, minéralogique, biostratigraphique, géochimique organique et minérale. Ministère de l'Énergie et des Ressources, Québec, DP-0256, 40p.

INRS-Pétrole 1976. Forage New Associated Consolidated Paper – Anticosti no. 1 (49°37'20'' - 63°26'20'': 5770 pieds). Stratigraphie, potential roche-mère et diagenèse minérale et organique. Ministère de l'Énergie et des Ressources, Québec, DPV-0361 (F-E), 78p.

Jacob, H. 1985. Disperse solid bitumens as an indicator for migration and maturity in prospecting for oil and gas. Erdol Und Kohle, v. 38 p. 365–366.

Jarvie, D.M., 2012a. Shale resource systems for oil and gas: part 2 - Shale-oil resource systems. In: Breyer, J.A. (ed.), Shale Reservoirs-Giant Resources for the 21st Century, AAPG Memoir, 97, p. 89-119.

Jarvie, D. M., 2012b, Shale resource systems for oil and gas: Part 1—Shale-gas resource systems, in J. A. Breyer, J.A. (Ed.), Shale reservoirs—Giant resources for the 21st century, AAPG Memoir 97, p. 69–87.

Journel, A. G., 2013, Fundamentals of Geostatistics in five lessons, Published by the American Geophysical Union as part of the Short Courses in Geology Series, Volume 8. Print ISBN: 9780875907086, Online ISBN: 9781118667606, DOI: 10.1029/SC008

Lavoie, D., 2008. Appalachian Foreland Basin in Canada, In: K.J. Hsü, A.D. Miall, (eds.), Sedimentary Basins of the World, series ed. Sedimentary Basins of the World — USA and Canada, vol. 5. Elsevier Science, p. 65–103.

Lavoie, D., Chi, G., 2010. Lower Paleozoic foreland basins in eastern Canada: tectono-thermal events recorded by faults, fluids and hydrothermal dolomites. Bulletin of Canadian Petroleum Geology, v. 58, p 17-35.

Lavoie, D., Chi, G., Brennan-Alpert, P., Desrochers, A., Bertrand, R., 2005. Hydrothermal dolomitization in the Lower Ordovician Romaine Formation of the Anticosti Basin: significance for hydrocarbon exploration: Bulletin of Canadian Petroleum Geology, v. 53, p. 454-472.

Lavoie, D., Pinet, N., Dietrich, J., Hannigan, P., Castonguay, S., Hamblin, A. P., Giles, P., 2009. Petroleum resource assessment, Paleozoic successions of the St. Lawrence Platform and Appalachians of eastern Canada. Geological Survey of Canada, Open File 6174, 275p.

Lavoie, D., Obermajer, M., Fowler, M., 2011. Rock-eval/TOC data from Cambrian–Ordovician St. Lawrence Platform and Humber Zone and Silurian–Devonian Gaspé Belt successions, Quebec. Geological Survey of Canada, Open File 6050.

Lavoie, D., Desrochers, A., Dix, G., Knight, I., Salad Hersi, O., 2012. The great American carbonate bank in eastern Canada: an overview. In: Derby, J.R., Fritz, R.D., Longacre, S.A., Morgan, W.A., Sternbach,

C.A. (Eds.), The Great American Carbonate Bank: The Geology and Economic Resources of the Cambrian–Ordovician Sauk Megasequence of Laurentia: AAPG Memoir. 98, p. 499–523.

Lavoie, D., Rivard, C., Lefebvre, R., Séjourné, S., Thériault, R., Duchesne, M. J., Ahad, J. M. E., Wang, B., Benoit, N., Lamontagne, C., 2014. The Utica Shale and gas play in southern Quebec : Geological and hydrogeological syntheses and methodological approaches to groundwater risk evaluation. International Journal of Coal Geology, v.126, p.77-91.

Long, D.G.F., 2007. Tempestite frequency curves: a key to Late Ordovician and Early Silurian subsidence, sea-level change and orbital forcing in the Anticosti foreland basin, Quebec, Canada. Canadian Journal of Earth Sciences, v. 44, p. 413-431.

Lynch, G., 2001. Shell Canada – Encal Energy, Anticosti Island Exploration 1997-2000. Ministère des Ressources Naturelles et de la Faune du Québec, Report 2000TD456-01, 32 p.

Lynch, G., Grist, A.M., 2002. Thermal modelling of the Laurentian margin beneath Anticosti Island using AFTA, 1D well profiles and bulk fluid inclusions. Canadian Society of Petroleum Geologists, Annual meeting, Calgary 2012. Program with abstracts.

Marcil, J.S., Dorrins, P.K., Lavoie, J., Mechti, N., 2014. Anticosti Island, Québec : Compelling data for deep fairway Utica-Equivalent oil. Unconventional resources technology conference 2014, paper SPE-2014-1931192. Denver, Colorado.

Milici, R.C., 2005. Assessment of Undiscovered Natural Gas Resources in Devonian Black Shales, Appalachian Basin, Eastern U.S.A. U.S. Geological Survey Open-File Report 2005-1268.

Momper, J. A., 1978, Oil migration limitations suggested by geological and geochemical considerations. In: W. H. Roberts and R. J. Cordel, (eds.), Physical and Chemical Constraints on Petroleum Migration: AAPG Continuing Education Course Notes Series no. 8, p. B1–B60

Mossop, G.D., Wallace-Dudley, K.E., Smith, G.G., Harrison, J.C., 2004. Sedimentary basins of Canada, Geological Survey of Canada, Open File 4673, 1 sheet.

Passey, Q.R., Creaney, S., Kulla, J.B., Moretti F.J., Stroud, J.D. 1990. A practical model for organic richness from porosity and resistivity logs. AAPG Bulletin, v. 74, p. 1777-1794.

Passey, Q.P., Bohacs,K.M., Esch,W.L., Klimentidis, R., and Sinha, S., 2010, From oil-potential source rock to gas-producing shale reservoir, - geological and petrophysical characterization of unconventional shale-gas reservoirs. SPE 131350.

Pepper, A. S., Dodd, T. A., 1995. Simple kinetic models of petroleum formation. Part II: oil-gas cracking. Marine and Petroleum Geology, Vol. 12, No. 3, pp. 321-340, 1995.

Pinet, N., Keating, P., Lavoie, D., Dietrich, J., Duchesne, M.J., Brake, V., 2012. Revisiting the Appalachian structural front and offshore Anticosti Basin (northern Gulf of St. Lawrence, Canada) by integrating old and new geophysical datasets. Marine and Petroleum Geology, v. 32, p. 50-62.

Pinet. N., Brake, V, Lavoie, D., 2015. Geometry and regional significance of joint sets in the Ordovician-Silurian Anticosti Basin: new insights from fracture mapping. Geological Survey of Canada, Open File 7752, 26 p.

Ramm M., 1991. Porosity – depth trends in reservoir sandstones: theoretical models related to Jurassic sandstone offshore Norway. Marine and Petroleum Geology, v. 9 p. 553-567.

Riva, J., 1969. Middle and Upper Ordovician graptolites faunas of the St. Lawrence Lowlands of Quebec and Anticosti Island. In: Kay, G.M. (Ed.), North Atlantic Geology and Continental Drift. American Association of Petroleum Geologists, Memoir, 12, pp. 513–556.

Rokosh, C.D., Lyster, S., Anderson, S.D.A., Beaton, A.O., Berhane, H., Brazzoni, T., Chen, D., Cheng, Y., Mack, T., Pana, C. and Pawlowicz, J.G., 2012. Summary of Alberta's shale and siltstone-hosted resource potential. Energy Resources Conservation Board, ERCB/AGS Open File Report 2012-6.

Sami, T., Desrochers, 1992. Episodic sedimentation on an early Silurian, storm-dominated carbonate ramp, Becscie and Merrimack formations, Anticosti Island, Canada. Sedimentology, v. 39, p. 355-381.

Sanford, B.V., 1993. St. Lawrence Platform- Geology. In: D.F.,\ Scott, and J.D. Aitken, (eds.), Sedimentary Cover of the Craton in Canada, Geological Survey of Canada, Geology of Canada, v. 5, p. 723-786.

Schuchert, C., Twenhofel, W.H., 1910. Ordovician–Silurian section of the Mingan and Anticosti islands, Gulf of Saint Lawrence. Geological Society of America Bulletin 21, 677–716.

Séjourné, S., 2015a. Étude géomécanique de la Formation de Macasty et de sa couverture dans un puits pétrolier et gazier (Pétrolia/Corridor Chaloupe No. 1), Île d'Anticosti, Québec. Commission géologique du Canada, Dossier Public 7892, 52p.

Séjourné, S., 2015b. Étude géomécanique régionale de la Formation de Macasty et de sa couverture d'après les puits pétroliers et gaziers de l'Île d'Anticosti, Québec. Commission géologique du Canada, Dossier public 7907, 114p.

Séjourné, S., Malo, M., 2015. Géologie et potentiel en hydrocarbures des bassins sédimentaires du sud du Québec. INRS-ETE - Rapport de recherche, R1552. Ministère de l'Énergie et des Ressources Naturelles, 147p.

Suárez-Ruiz, I., Flores, D., Filho, J.G.M., Hackley, P.C., 2012. Review and update of the applications of organic petrology: part 1, geological applications. International Journal of Coal Geology, v. 99, p. 54–112.

Tissot, B. P., Pelet, R., Ungerer, P., 1987. Thermal history of sedimentary basins, maturation indices, and kinetics of oil and gas generation. AAPG Bulletin, v. 71, p. 1445-1466.

Thériault, R., 2012. Caractérisation du Shale d'Utica et du Groupe de Lorraine, Basses-Terres du Saint-Laurent — Partie 2: Interprétation géologique. Ministère des Ressources naturelles et de la Faune. (SIGEOM, DV 2012-04, 80 pp.).

U.S. Energy Information Administration, 2011. Review of Emerging Resources: US Sale gas and shale oil plays, 82 p.

U.S. Energy Information Administration, 2013. Technically recoverable shale gas and shale oil resources, p. updated in 2015: https://www.eia.gov/analysis/studies/worldshalegas/

Wang, P., Chen, Z., Pang, X., K. Hu, M. Sun and X. Chen, 2016. Revised models for determining TOC in shale play: Example from Devonian Duvernay shale, Western Canada Sedimentary Basin, Marine and Petroleum Geology, v.70. P. 304-319, http://dx.doi.org/10.1016/j.marpetgeo.2015.11.023

Wickstrom, L., 2013. Geology and activity of the Utica-Point Pleasant of Ohio. Tulsa Geological Society presentation. Search and Discovery Article #10490 (2013).

Wilson, J.L., Fritz, R.D., Medlock, P.L., 1991, The Arbuckle Group-relationship of core and outcrop analyses to cyclic stratigraphy and correlation. In K.S. Johnson, (ed.), Arbuckle Core Workshop and Field Trip: Oklahoma Geological Survey, Special Publication 91-3, p. 133-144.

Zou, Y.-R., Peng, P., 2001. Overpressure retardation of organic-matter maturation: a kinetic model and its application. Marine and Petroleum Geology, v. 18, p. 707-713.